J Physiol 591.17 (2013) pp 4149–4166

The Journal of Physiology

Stabilization of Kv4 protein by the accessory K^+ channel interacting protein 2 (KChIP2) subunit is required for the generation of native myocardial fast transient outward K^+ currents

Nicholas C. Foeger, Wei Wang, Rebecca L. Mellor and Jeanne M. Nerbonne

Department of Developmental Biology, Washington University Medical School, St. Louis, MO 63110, USA

Key points

- The cytosolic K^+ channel accessory subunit, K^+ channel interacting protein 2 (KChIP2), was previously suggested to be critical in the generation of cardiac fast transient outward current ($I_{to,f}$) channels.
- The experiments presented here revealed the novel finding that targeted deletion of KChIP2 results in the complete *loss* of the Kv4.2 protein, although *Kcnd2* (Kv4.2) transcript expression is not decreased in KChIP2$^{-/-}$ ventricles.
- In contrast, the slow transient outward current, $I_{to,s}$, is increased in KChIP2$^{-/-}$ left ventricular apex myocytes and ventricular action potential waveforms in KChIP2$^{-/-}$ and WT mice are not significantly different.
- These results demonstrate the critical role of KChIP2 in the stabilization of native Kv4 proteins and that the loss of the Kv4.2 protein underlies the *elimination* of $I_{to,f}$ in KChIP2$^{-/-}$ myocytes.
- Taken together, the results here demonstrate that electrical remodelling compensates for the *elimination* of $I_{to,f}$, maintaining physiological action potential repolarization in mouse myocardium.

Abstract The fast transient outward K^+ current ($I_{to,f}$) underlies the early phase of myocardial action potential repolarization, contributing importantly to the coordinated propagation of activity in the heart and to the generation of normal cardiac rhythms. Native $I_{to,f}$ channels reflect the tetrameric assembly of Kv4 pore-forming (α) subunits, and previous studies suggest roles for accessory and regulatory proteins in controlling the cell surface expression and the biophysical properties of Kv4-encoded $I_{to,f}$ channels. Here, we demonstrate that the targeted deletion of the cytosolic accessory subunit, K^+ channel interacting protein 2 (KChIP2), results in the complete *loss* of the Kv4.2 protein, the α subunit critical for the generation of mouse ventricular $I_{to,f}$. Expression of the *Kcnd2* (Kv4.2) transcript in KChIP2$^{-/-}$ ventricles, however, is unaffected. The loss of the Kv4.2 protein results in the elimination of $I_{to,f}$ in KChIP2$^{-/-}$ ventricular myocytes. In parallel with the elimination of $I_{to,f}$, the slow transient outward K^+ current ($I_{to,s}$) is upregulated and voltage-gated Ca^{2+} currents ($I_{Ca,L}$) are decreased. In addition, surface electrocardiograms and ventricular action potential waveforms in KChIP2$^{-/-}$ and wild-type mice are not significantly different, suggesting that the upregulation of $I_{to,s}$ and the reduction in $I_{Ca,L}$ compensate for the loss of $I_{to,f}$. Additional experiments revealed that $I_{to,f}$ is not 'rescued' by adenovirus-mediated expression of KChIP2 in KChIP2$^{-/-}$ myocytes, although $I_{Ca,L}$ densities are increased. Taken together, these results demonstrate that association with KChIP2 early in the biosynthetic pathway

DOI: 10.1113/jphysiol.2013.255836

and KChIP2-mediated stabilization of Kv4 protein are critical determinants of native cardiac $I_{to,f}$ channel expression.

(Received 26 March 2013; accepted after revision 23 May 2013; first published online 27 May 2013)

Corresponding author J. M. Nerbonne: Department of Developmental Biology, Washington University School of Medicine, Campus Box 8103, 660 South Euclid Avenue, St. Louis, MO 63110, USA. Email: jnerbonne@wustl.edu

Abbreviations α, pore-forming; α-, anti-; 4-AP, 4-aminopyridine; APA, action potential amplitude; APD_{20}, action potential duration at 20% recovery; APD_{50}, action potential duration at 50% recovery; APD_{90}, action potential duration at 90% recovery; EGFP, enhanced green fluorescent protein; ES, embryonic stem; HPRT, hypoxanthine-guanine phosphoribosyltransferase; I_{Ca}, voltage-gated inward Ca^{2+} currents; $I_{Ca,L}$, L-type Ca^{2+} current; I_{K1}, inwardly rectifying K^+ current; $I_{K,slow}$, slow-inactivating outward K^+ current; I_{peak}, peak outward K^+ current; I_{ss}, non-inactivating steady-state outward K^+ current; $I_{to,f}$, fast transient outward K^+ current; $I_{to,s}$, slow transient outward K^+ current; KChIP, K^+ channel interacting protein; $KChIP2^{-/-}$, KChIP2 targeted deletion; Kir, inward rectifier K^+; Kv, voltage-gated K^+; $Kv4.2^{-/-}$, Kv4.2 targeted deletion; Kv4.2DN, Kv4.2 dominant negative; LVA, left ventricular apex; m.o.i., multiplicity of infection; NCS-1, neuronal calcium sensor 1; τ_{decay}, decay time constant; τ_{rec}, inactivation recovery time constant; TransR, transferrin receptor; WT, wild type.

Introduction

Voltage-gated K^+ (Kv) channels are the primary determinants of action potential repolarization in cardiac myocytes, and in most cardiac cells, multiple types of Kv channels that subserve this function are co-expressed (Nerbonne & Kass, 2005). Increasing evidence suggests that native Kv channels function in macromolecular protein complexes comprising pore-forming (α) and accessory subunits, as well as additional regulatory, signalling and cytoskeletal proteins (Petrecca *et al.* 2000; Nerbonne & Kass, 2005; Dai *et al.* 2009; Norris *et al.* 2010*b*; Marionneau *et al.* 2011; Nerbonne, 2011). Considerable evidence has accumulated, for example, to suggest that the channels which generate the fast transient outward K^+ current ($I_{to,f}$), which underlies phase 1 repolarization and contributes importantly to the normal propagation of activity in the ventricular myocardium (Antzelevitch *et al.* 1991; Greenstein *et al.* 2000; Sun & Wang, 2005; Niwa & Nerbonne, 2010), reflect the heteromeric assembly of α subunits of the Kv4 subfamily together with the K^+ channel accessory protein, K^+ channel interacting protein 2 (KChIP2; Kuo *et al.* 2001; Guo *et al.* 2002) and other cytosolic (Aimond *et al.* 2005) and transmembrane accessory subunits (Radicke *et al.* 2005, 2006; Roepke *et al.* 2008; Niwa & Nerbonne, 2010).

Previous studies have demonstrated that Kv4.2 is the critical α subunit required for the expression of functional $I_{to,f}$ channels in mouse ventricular myocytes (Guo *et al.* 2005). Targeted deletion of Kv4.2, for example, eliminates $I_{to,f}$ in ($Kv4.2^{-/-}$) mouse ventricular myocytes (Guo *et al.* 2005), whereas deletion of Kv4.3 does not measurably affect mouse ventricular $I_{to,f}$ densities (Niwa *et al.* 2008). The elimination of $I_{to,f}$ in $Kv4.2^{-/-}$ ventricular myocytes (Guo *et al.* 2005) and in myocytes isolated from animals expressing a mutant Kv4.2 subunit (Kv4.2DN) that functions as a dominant negative (Barry *et al.* 1998; Guo *et al.* 2000) results in increased expression of the Kv1.4-encoded slow transient outward Kv current, $I_{to,s}$. It has also been reported that $I_{to,f}$ is eliminated in ventricular myocytes from (*KChIP2*$^{-/-}$) mice harbouring a targeted disruption of the *Kcnip2* (KChIP2) locus (Kuo *et al.* 2001; Thomsen *et al.* 2009*a*), although the molecular mechanism(s) responsible for the KChIP2-mediated loss of $I_{to,f}$ were not defined.

Recent findings led us to hypothesize that these observations were consistent with a critical regulatory role for KChIP2 in the stabilization of Kv4 protein and, therefore, with an absolute requirement for KChIP2 in the generation of native Kv4-encoded channels. More specifically, recent studies in heterologous cells, we demonstrated that KChIP2 co-expression markedly increases total Kv4.2 protein expression (Foeger *et al.* 2010) as well as modifying Kv4.2 current densities and properties (An *et al.* 2000; Bähring *et al.* 2001; Shibata *et al.* 2003). Further experiments revealed a critical role for the N-terminal 23 amino acids in Kv4.2 in mediating the association with KChIP2, findings consistent with predictions based on structural analysis of Kv4-KChIP complexes (Pioletti *et al.* 2006; Wang *et al.* 2007) and, in addition, that the binding of KChIP2 to Kv4.2 stabilizes both proteins (Foeger *et al.* 2010).

To explore directly the hypothesis that KChIP2 is required for the *in vivo* stabilization of myocardial Kv4.2 protein expression, we generated ($KChIP2^{-/-}$) mice harbouring a targeted disruption of the *Kcnip2* (KChIP2) locus. Consistent with our hypothesis, biochemical studies revealed that the targeted deletion of KChIP2 results in the *loss* of Kv4.2 protein in adult mouse ventricles, whereas *Kcnd2* transcript expression is unaffected. The loss of the Kv4.2 protein is reflected in the elimination of $I_{to,f}$ in $KChIP2^{-/-}$ ventricular myocytes. Consistent with previous findings in $Kv4.2^{-/-}$ and Kv4.2DN animals, further analyses revealed the upregulation of $I_{to,s}$ in $KChIP2^{-/-}$ ventricular myocytes and the normalization of ventricular action potential waveforms and repolarization.

Methods

Ethical approval

Animals were handled in accordance with the NIH Guide for the Care and Use of Laboratory Animals. All protocols involving animals were approved by the Animal Studies Committee at Washington University Medical School. Experiments were performed on adult (8–15 weeks) KChIP2$^{-/-}$, Kv4.2$^{-/-}$ (Guo *et al.* 2005) and wild-type (WT) C57BL6/J mice. A total of 21 KChIP2$^{-/-}$, two Kv4.2$^{-/-}$ and 25 WT mice were used for the electrophysiological ($n = 30$), biochemical ($n = 6$) and transcript ($n = 12$) analyses presented here.

Generation of the *Kcnip2* (KChIP2) targeting construct

A targeting construct in a modified pSV/Lox-neo-lox vector (a gift from Dr Joshua R. Sanes, Harvard University) was generated to produce disruption of the *Kcnip2* gene and the generation of KChIP2$^{-/-}$ mice. The pSV/Lox-neo-lox vector contains both a neomycin-resistance cassette and the diphtheria toxin gene to facilitate the selection of embryonic stem (ES) cells that have incorporated the targeting vector through homologous recombination. Mouse genomic DNA, isolated from the 129x1/SvJ mouse strain, was obtained from the Jackson Laboratory (Bar Harbor, ME, USA). Following the strategy described by Kuo *et al.* (2001) to generate *KChIP2*$^{-/-}$ mice, a 4.0 kb fragment of mouse *Kcnip2*, upstream of exon 4, was generated by PCR and cloned into the pSV/Lox-neo-lox vector between the *Asc*I and *Sal*I restriction sites. Additionally, a 1.6 kb fragment of mouse *Kcnip2* downstream of exon 9 was generated by PCR and cloned into the pSV/Lox-neo-lox vector between the *Age*I and *Pac*I restriction sites. In the resulting targeting construct (see Fig. 1*A*), exons 4–9 in *Kcnip2* are replaced with the neomycin resistance gene. In the targeted allele, therefore, the sequence coding the majority of the KChIP 'core' domain (An *et al.* 2000) is removed, resulting in a null allele that does not yield any full-length or truncated KChIP2 message/protein (see Fig. 1*A*).

Generation of KChIP2 knock-out (KChIP2$^{-/-}$) mice

ES cells of the 129/Sv(R1) line were electroporated with the (linearized) *Kcnip2* targeting vector by the Washington University ES Cell Core, supported by NIH grant P60 DK020579 to the Diabetes Research Center. Cells were selected for neomycin resistance using G418 and 144 colonies were picked for Southern blot analysis. Genomic Southern analysis using 5′ and 3′ probes (see Fig. 1*A*) flanking the targeted insertion identified three positive clones that underwent homologous recombination to incorporate the neomycin cassette in place of exons 4–9 in KChIP2 (Fig. 1*B*).

The three ES-positive clones were injected into C57BL6/J blastocysts in the Washington University Transgenic Mouse Core, and chimeric mice were obtained. Male coat-colour chimeras (of 80–90%) were selected, and subsequently bred with WT (C57BL6/J) females to obtain F1 heterozygotes. Germline transmission was obtained from three of these (chimeras), and the offspring of these mice were intercrossed to generate F2 homozygotes for initial analysis. Southern blots using the 5′ and 3′ *Kcnip2* probes were performed to genotype the offspring (Fig. 1*C*). Heterozygous (F1) animals were bred into the C57BL6/J background for 10 generations prior to being crossed to generate C57BL6/J KChIP2$^{-/-}$ homozygotes, again identified by Southern blot analysis.

Plasmid construct and viral vector generation

The coding sequence for the red fluorescent protein tdTomato (Shaner *et al.* 2004; a gift from Dr Roger Y. Tsien, University of California at San Diego) was cloned in the multiple cloning site of the pBK-CMV phagemid vector (Stratagene, La Jolla, CA, USA) between the *Nhe*I and *Not*I restriction sites to generate pBK-CMV.tdTomato. The AdEGI vector (Johns *et al.* 1999; a gift from Dr David C. Johns, Johns Hopkins University) is a bi-cistronic adenoviral shuttle vector expressing enhanced green fluorescent protein (EGFP) and a second open reading frame separated by an internal ribosomal entry site in a single transcript driven by the ecdysone promoter. A *Not*I restriction site was introduced into AdEGI at base pair 2498 (following EGFP) by site-directed mutagenesis using the QuikChange XL kit (Stratagene) with the following primers: 5′-GAGC TGTACAAGTGCGGCCGCTAGTACT CCGGT and 3′-ACCGGAGTACTAGCGGCCGCACTTG TACAGCTC. This construct was then digested with *Nhe*I and *Not*I restriction endonucleases to excise the EGFP, and tdTomato was subcloned into the *Nhe*I and *Not*I sites to generate the vector AdloxERI. Subsequently, the coding sequence for *KCNIP2* (NM_173192), encoding human KChIP2, was cloned into the AdloxERI vector at the *Xho*I and *Sac*I restriction sites to generate the vector AdloxERI.hKChIP2. Recombinant adenovirus vectors encoding tdTomato or tdTomato plus KChIP2 were generated from AdloxERI and AdloxERI.hKChIP2, respectively, using previously described methods (Johns *et al.* 1999).

Electrophysiological recordings

Surface electrocardiograms (ECGs) were recorded from anaesthetized (tribromoethanol, Avertin; 0.25 mg kg^{-1}, I.P.; Sigma, St Louis, MO, USA) KChIP2$^{-/-}$ and WT mice,

using needle electrodes connected to a dual bioamplifier (PowerLab 26T, AD Instruments, Colorado Springs, CO, USA). ECG signals were acquired for 2 min, stored and analysed offline using the LabChart 7.1 (AD Instruments) software; lead II recordings were analysed. In each record, the QT interval was determined as the time interval between the initiation of the QRS complex and the end of the T wave, defined as the time the negative deflection of the T wave returned to the baseline. The measurement is illustrated in Fig. 7. QT intervals were corrected for heart rate using the formula $QTc = QT/(\sqrt{RR}/100)$ (Mitchell *et al.* 1998).

Myocytes were isolated from adult (8–15 weeks old) WT and KChIP2$^{-/-}$ animals using described procedures (Xu *et al.* 1999*b*; Brunet *et al.* 2004). Briefly, hearts were removed from animals anaesthetized using 2.5% halothane inhalation, mounted on a Langendorf apparatus and perfused retrogradely through the aorta with 25 ml of (0.8 mg ml^{-1}) collagenase-containing (type II, Worthington Biochemical Corp., Lakewood, NJ, USA) solution (Xu *et al.* 1999*b*; Brunet *et al.* 2004). Following the perfusion, the left ventricular apex (LVA) and interventricular septum were separated using a fine scalpel and iridectomy scissors, mechanically dispersed, plated on laminin-coated coverslips and maintained in a 95% air/5% CO_2 incubator.

For experiments aimed at examining the functional effects of KChIP2 reintroduction in KChIP2$^{-/-}$ myocytes, the whole ventricle was mechanically dispersed, plated on laminin-coated coverslips. Following cell adherence, the culture medium was replaced with medium containing recombinant adenovirus encoding either tdTomato or toTomato plus KChIP2 together with a second virus which encodes the ecdysone receptor (AdVgRXR) which binds muristerone A (Johns *et al.* 1999). Based on preliminary dose–response experiments (data not shown), myocytes were infected with virus at a multiplicity of infection (m.o.i.) of ∼5000 for the test virus and ∼500 for the ecdysone receptor virus, resulting in >95% of myocytes expressing detectable tdTomato after 36 h with minimal cell death (compared with uninfected cells from the same isolation). After 2 h, the infection medium was replaced with culture medium supplemented with 0.5 mM muristerone A (to induce gene expression) for 36 h before electrophysiological recordings were obtained. The dose of muristerone A was selected to activate the receptor maximally on the basis of preliminary dose–response curves (data not shown).

Whole-cell current- and voltage-clamp recordings were obtained from uninfected LVA and interventricular septum myocytes within 12 h of isolation at room temperature (22–23°C) or at physiological temperature (35–37°C). Voltage-clamp recordings were also obtained at room temperature from ventricular cells 36–48 h following adenoviral infection. Voltage- and current-clamp experiments were controlled and data were collected using an Axopatch 1D (Molecular Devices, Sunnyvale, CA, USA) or a Dagan 3900A (Dagan Corp., Minneapolis, MN, USA) patch clamp amplifier interfaced to a microcomputer with a Digidata 1332 analog/digital interface and the pCLAMP9 software package (Molecular Devices). Data were filtered at 5 kHz before storage.

For recordings of whole-cell K^+ currents, pipettes contained (in mM): KCl 135, EGTA 10, Hepes 10 and glucose 5 (pH 7.2; 310 mOsm). The bath solution contained (in mM): NaCl 136, KCl 4, $MgCl_2$ 2, $CaCl_2$ 1, $CoCl_2$ 5, tetrodotoxin (TTX) 0.02, Hepes 10 and glucose 10 (pH 7.4; 300 mOsm). For recordings of whole-cell voltage-gated Ca^{2+} (I_{Ca}) currents, the $CoCl_2$ was omitted from the bath and the KCl in the pipette and bath solutions was replaced with CsCl (140 mM) and TEA-Cl (4 mM), respectively. The TTX and the $CoCl_2$ were omitted from the bath solution for current-clamp recordings. Whole-cell voltage-gated K^+ (Kv) currents were recorded in response to 4.5 or 20 s voltage steps to test potentials between −60 and +60 mV from a holding potential (HP) of −70 mV. Currents (I_{K1}) through inward rectifier K^+ (Kir) channels, evoked in response to (4.5 s) hyperpolarizations to −120 mV from the same HP, were also recorded in each cell. Whole-cell voltage-gated inward Ca^{2+} currents (I_{Ca}) were evoked in response to 400 ms voltage steps to test potentials between −40 and +50 mV from a prepulse to −40 mV, presented from the same holding potential (−70 mV) to inactivate voltage-gated Na^+ currents. Action potentials were elicited in response to brief (2–5 ms) depolarizing current injections of varying amplitudes, delivered at 1 Hz for the recordings at room temperature or at 10 Hz for recordings at physiological temperature. Action potential recordings were obtained after the waveforms reached a steady state, typically 10 beats.

Voltage-clamp and current-clamp data were compiled and analysed using Clampfit (Version 9.2, Molecular Devices) and Excel (Microsoft, Redmond, WA, USA). Integration of the capacitative transients, recorded during brief ± 10 mV voltage steps from the holding potential (−70 mV) provided whole-cell membrane capacitances (C_m). Leak currents were always <200 pA, and were not corrected. Series resistances (<10 MΩ) were routinely compensated for electronically (>80%). Voltage errors resulting from the uncompensated series resistances were ≤8 mV and were not corrected. The input resistances of adult mouse WT ($n = 37$) and KChIP2$^{-/-}$ ($n = 12$) LVA myocytes and of WT ($n = 20$) and KChIP2$^{-/-}$ ($n = 8$) interventricular septum myocytes were not significantly different, with mean ± SEM values of 656 ± 112, 576 ± 148, 544 ± 109 and 418 ± 135 MΩ, respectively. Resting membrane potentials, action potential amplitudes

and action potential durations at 20, 50 and 90% repolarization were also measured.

Peak Kv current, I_{K1} and I_{Ca} amplitudes were measured as the maximal amplitudes of the outward or inward currents evoked at each test potential, and normalized to whole-cell membrane capacitances (in the same cell) to provide current densities (in pA pF^{-1}). Using previously described methods (Xu *et al.* 1999*b*; Brunet *et al.* 2004; Guo *et al.* 2005), the decay phases of the outward currents, recorded from WT and KChIP2$^{-/-}$ LVA and interventricular septum myocytes during 4.5 s depolarizing voltage steps at room temperature, were analysed to provide the time constants of inactivation (τ_{decay}) and the amplitudes of $I_{to,f}$, $I_{to,s}$, $I_{K,slow}$ and I_{ss}. Consistent with previously published data (Xu *et al.* 1999*b*; Brunet *et al.* 2004), three exponentials (reflecting $I_{to,f}$, $I_{to,s}$ and $I_{K,slow}$) were required to fit the decay phases of the Kv currents in most (~80%) of the WT cells from the interventricular septum, whereas the decay phases of the Kv currents in WT LVA cells and KChIP2$^{-/-}$ LVA and septum cells were well described by two exponentials reflecting $I_{to,f}$ and $I_{K,slow}$ (WT) and $I_{to,s}$ and $I_{K,slow}$ (KChIP2$^{-/-}$), respectively. Analyses of the Kv currents evoked during 20 s depolarizations at room temperature further allowed the resolution of the time constants of inactivation and the amplitudes of the two components of $I_{K,slow}$, $I_{K,slow1}$ and $I_{K,slow2}$, as described previously by Liu *et al.* (2011). The waveforms of the outward Kv currents in WT and KChIP2$^{-/-}$ LVA myocytes recorded at physiological temperatures were best described by the sum of three exponentials, corresponding to $I_{to,f}$ (or $I_{to,s}$), $I_{K,slow1}$ and $I_{K,slow2}$, as described in the text.

Transcript analyses

Total RNA was isolated from left ventricles, right ventricles and interventricular septa of WT ($n = 6$) and KChIP2$^{-/-}$ ($n = 6$) hearts with Trizol and subsequently DNase treated using described methods (Guo *et al.* 2005; Marionneau *et al.* 2008). RNA concentrations were determined by optical density measurements. Transcript analyses of genes encoding ion channel pore-forming (α) and accessory subunits, as well as of the control gene hypoxanthine-guanine phosphoribosyltransferase (*Hprt*), were carried out using SYBR green RT-PCR in a two-step process (Guo *et al.* 2005; Marionneau *et al.* 2008). Primers used were previously validated for specificity and are listed in Table 1. Data were analysed using the threshold cycle (C_T) relative quantification method. The expression of each transcript was normalized to the expression of *Hprt* in the same sample. Each value for each transcript was then expressed relative to the mean value (for the same transcript) of the WT samples; means ± SEM normalized values are presented.

Biochemical analyses

Protein lysates were prepared from whole ventricles of WT and KChIP2$^{-/-}$ animals using described methods (Diwan *et al.* 2007, 2009). Briefly, ventricles from individual animals were harvested and homogenized (separately) in ice-cold lysis buffer containing (in mM): Hepes 10 (pH 7.2), sucrose 320, $MgCl_2$ 3, $Na_2P_4O_7$ 25, dithiothreitol 1, EGTA 5, NaF 20, Na_3VO_4 2 with protease inhibitor cocktail tablet (Roche, Mannheim, Germany). Samples were centrifuged at 1000 *g* for 20 min at 4°C to remove nuclei and myofibrils. The supernatants were then centrifuged at 10,000 *g* for 20 min at 4°C, and the resultant pellets, containing rough endoplasmic reticulum and mitochondria, were discarded. The supernatants from the 10,000 *g* centrifugation step were then centrifuged at 100,000 *g* for 1 h at 4°C; supernatants from this centrifugation step, containing cytoplasmic proteins, were discarded. The resultant pellets (100 bp fractions) were resuspended in phosphate-buffered saline (in mM: NaCl 136, KCl 2.6, NaH_2PO_4 10, KH_2PO_4 1.7 (pH 7.4)) containing protease inhibitor cocktail tablet (Roche) and Triton X-100 (1%).

For the isolation of brain tissue for biochemical analyses, mice were anaesthetized with isoflorane and decapitated and the brains rapidly removed. Cortices were dissected and flash frozen in liquid nitrogen. Tissue samples were homogenized in ice-cold lysis buffer containing (in mM) Tris 50 (pH 7.5), EDTA 1, NaCl 150 and Pefabloc 1, with 1 μg ml^{-1} pepstatin A (Calbiochem, Gibbstown, NJ, USA), protease inhibitor cocktail tablet (Roche), Halt phosphatase inhibitor cocktail (Pierce, Rockford, IL, USA) and Triton X-100 (1%).

Protein concentrations were determined using the BCA protein Assay Kit (Pierce). For Western blot analyses, 40 μg of the heart 100 bp fractions or 10 μg of the cortical lysates prepared from individual WT and KChIP2$^{-/-}$ mice (prepared as described above) were loaded on SDS-PAGE gels. The following commercially available antibodies were used: rabbit polyclonal anti-Kv4.2 (Sigma), mouse monoclonal anti-transferrin receptor (TransR) (Invitrogen, Carlsbad, CA, USA) and mouse monoclonal anti-GAPDH (Abcam, Cambridge, MA, USA). The mouse monoclonal anti-KChIP2 antibody was developed by and obtained from the UC Davis/NIH NeuroMab Facility, supported by NIH grant U24NS050606 and maintained by the University of California, Davis. The specificity of the polyclonal anti-Kv4.2 antibody was previously tested on protein extracts from Kv4.2$^{-/-}$ mice, in which the gene encoding Kv4.2 had been eliminated by homologous recombination (Guo *et al.* 2005); no signals corresponding to Kv4.2 were detected. The specificity of the Neuromab monoclonal anti-KChIP2 antibody is demonstrated here.

Table 1. Sequence-specific primers used in SYBR Green RT-PCR

Gene		Forward primer	Reverse primer
KChIP2	(*Kcnip2*)	5′-GGCTGTATCACGAAGGAGGAA	5′-CCGTCCTTGTTTCTGTCCATC
Kv4.2	(*Kcnd2*)	5′-GCCGCAGCACCTAGTCGTT	5′-CACCACGTCGATGATACTCATGA
Kv4.3	(*Kcnd3*)	5′-CCTAGCTCCAGCGGACAAGA	5′-CCACTTACGTTGAGGACGATCA
Kv1.4	(*Kcna4*)	5′-AGAGGCGGATGAACCCACTA	5′-GCCCACCAAAACGCATCT
NCS-1	(*Ncs1*)	5′-GTTCGCCACGTTTGTTTTCA	5′-GAGAACTCAATCCTGCCATCCT
Kv1.5	(*Kcna5*)	5′-AAAGTGTCACCTAAAGGCCAAGAG	5′-CCAGACAGAGGGCATACAGAGA
Kv2.1	(*Kcnb1*)	5′-CACACAGCAATAGCGTTCAACTT	5′-AGGCGTAGACACAGTTCGGC
TREK1	(*Kcnk2*)	5′-CCTTTTGTGCCCAGACTGTTTC	5′-GCAAAGCATTCAGATTCATTCATAG
TASK1	(*Kcnk3*)	5′-GCTTCCGCAACGTCTATGC	5′-GGGATGGAGTACTGCAGCTTCT
Cav1.2	(*Cacna1c*)	5′-CCCTTCTTGTGCTCTTCGTC	5′-ACACCCAGGGCAACTCATAG
HPRT	(*Hprt*)	5′-TGAATCACGTTTGTGTCATTAGTGA	5′-TTCAACTTGCGCTCATCTTAGG

After washing, membranes were incubated with a rabbit anti-mouse horseradish peroxidase-conjugated secondary antibody (Bethyl Laboratories, Montgomery, TX, USA) or a donkey anti-rabbit horseradish peroxidase-conjugated secondary antibody (GE Healthcare Life Sciences, Little Chalfont, UK) followed by SuperSignal West Dura Extended Duration substrate (Pierce). Signals were detected using a Molecular Imager Chemidoc XRS system running the Quantity One software, version 4.6 (Bio-Rad Laboratories, Hercules, CA, USA).

Statistical analyses

All averaged electrophysiological, molecular and biochemical data are presented as means ± SEM. The statistical significance of observed differences among cells/tissues/animals was evaluated using one-way analysis of variance (ANOVA), followed by *post hoc* Tukey's multiple comparison test. In some cases, the Student's *t* test was used to evaluate differences between groups. A two-tailed *P* value of <0.05 was considered statistically significant.

Results

Targeted disruption of the *Kcnip2* (KChIP2) locus

Testing our hypothesis that KChIP2 is required for the *in vivo* stabilization of myocardial Kv4.2 protein expression and the generation of native mouse ventricular $I_{to,f}$ channels required mice lacking KChIP2. Because the *KChIP2*$^{-/-}$ mouse line described by Kuo *et al.* (2001) was not available, a targeting construct was generated (Fig. 1*A*) in which exons 4–9 were replaced with a neomycin cassette, eliminating the majority of the C-terminal 'core' domain of the *Kcnip2* coding sequence (An *et al.* 2000), a strategy modelled after that described by Kuo *et al.* (2001). The core domain, which contains four Ca^{2+}-binding EF-hand domains, is highly conserved across KChIP family members (An *et al.* 2000; Pongs & Schwarz, 2010) and structural studies have demonstrated that the conserved KChIP core also contains a hydrophobic pocket which binds the N terminus of Kv4 α subunits (Pioletti *et al.* 2006; Wang *et al.* 2007). For screening ES cells and mice, 5′ and 3′ probes were designed (Fig. 1*A*) to distinguish between the targeted and endogenous *Kcnip2* sequences. Southern blot analysis of *Xmn*I-digested genomic DNA from ES cells that survived the selection procedure (see Methods) confirmed the presence of the targeted allele (Fig. 1*B*). The WT bands are at 11.7 kb (5′) and 11.2 kb (3′), and the bands corresponding to the targeted allele are at 13.9 kb (5′) and 6.3 kb (3′).

Blastocyst injections yielded three chimeric mice, two of which provided germline transmission on crossing with WT (C57BL6/J) mice. Congenic C57BL6/J (KChIP2$^{+/-}$) mice were bred to establish the KChIP2$^{-/-}$ line used here. Representative Southern blots with the 3′ and 5′ probes of tail DNA from the offspring of breeding KChIP2$^{+/-}$ animals are presented in Fig. 1*C*. The KChIP2$^{-/-}$ mice generated are viable and fertile and, on gross examination, are indistinguishable from WT mice. Gross histological examination of KChIP2$^{-/-}$ hearts also revealed no detectable differences from WT hearts. In addition, there was no evidence of cellular, tissue or whole animal pathology in older (16–23 weeks) KChIP2$^{-/-}$ animals. Western blot analyses, however, confirmed the loss of the KChIP2 protein in KChIP2$^{-/-}$ brains, whereas robust expression of KChIP2 is evident in WT brains (Fig. 1*D*).

Elimination of $I_{to,f}$ and Kv current remodelling in KChIP2$^{-/-}$ ventricular myocytes

Whole-cell voltage-clamp recordings obtained at room temperature (22–23°C) (Fig. 2) revealed that peak Kv current (I_{peak}) densities are significantly ($P < 0.01$) lower in myocytes isolated from the LVA of KChIP2$^{-/-}$ compared with WT mice (Table 2). Inwardly rectifying K^+ current (I_{K1}) densities in KChIP2$^{-/-}$ and WT LVA myocytes, by contrast, are indistinguishable (data not

shown). In addition, the waveforms of the Kv currents recorded at room temperature from WT and KChIP2$^{-/-}$ LVA myocytes are distinct (Fig. 2*A*). In particular, the rapid component of current decay, which reflects $I_{to,f}$ (Xu *et al.* 1999*b*; Brunet *et al.* 2004; Guo *et al.* 2005) and is prominent in WT LVA cells, is not evident in KChIP2$^{-/-}$ LVA myocytes (Fig. 2*B*; Table 2). Consistent with the elimination of $I_{to,f}$, the rapidly recovering current component ($I_{to,f}$), which is prominent in WT LVA myocytes (Barry *et al.* 1998; Guo *et al.* 2005), characterized by a recovery time

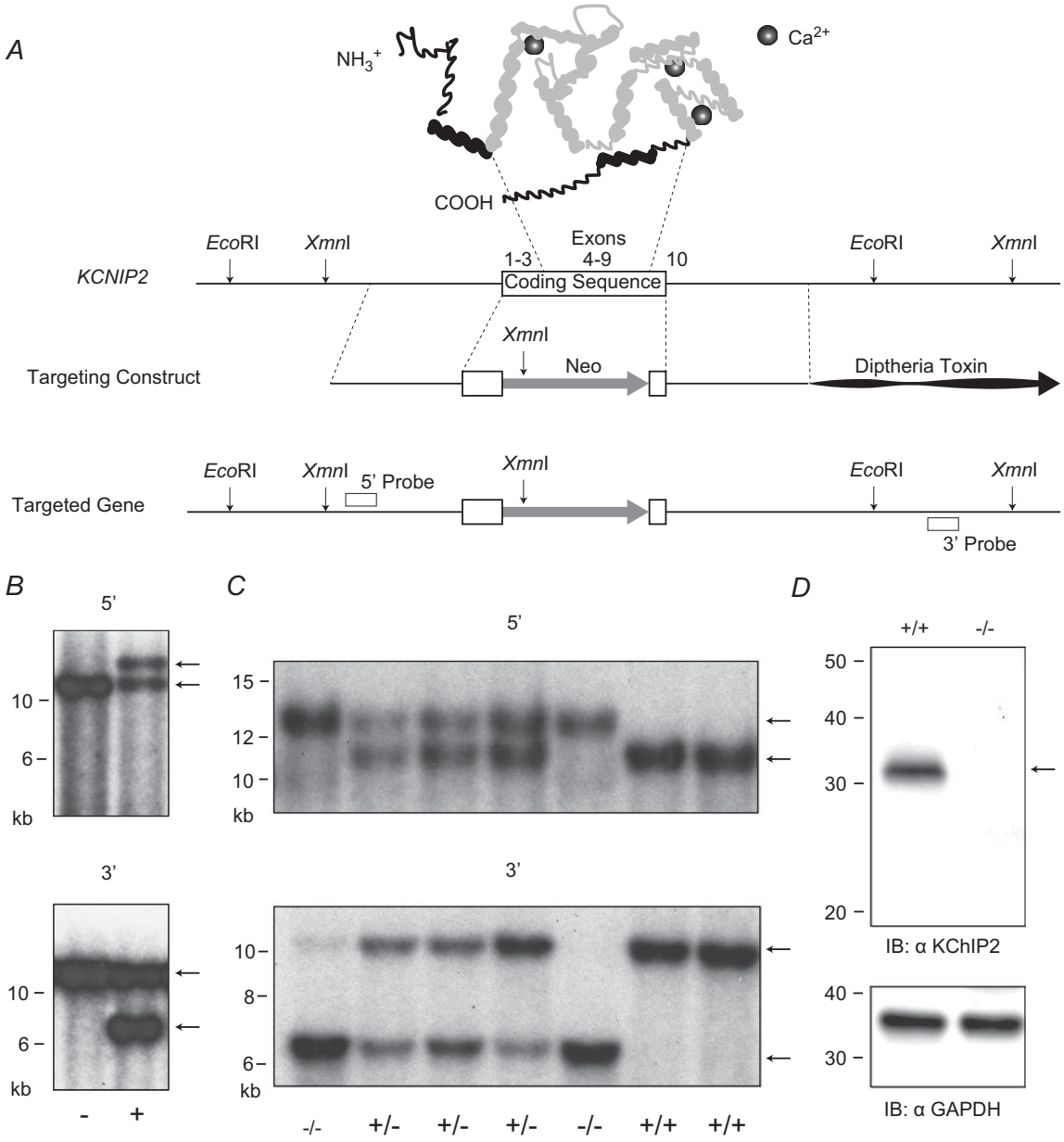

Figure 1. *Kcnip2* targeting construct and the generation of KChIP2$^{-/-}$ mice
A, the top schematic illustrates the general topography of KChIP2 and the approximate locations of Ca^{2+} binding (to the EF-hand motifs). Domains targeted for deletion are in grey and the physical maps of mouse *Kcnip2*, the targeting construct and the targeted allele are also illustrated. The regions selected for the generation of the 5′ and 3′ probes for Southern blot analysis are also indicated. *B*, *Xmn*I-digested genomic DNA from transfected ES cells that survived the selection procedure were screened using the 5′ and 3′ probes; results from a negative (left lane) and a positive (right lane) clone are depicted. *C*, Southern blots of genomic tail DNA from WT (KChIP2$^{+/+}$), homozygous targeted deletion (KChIP2$^{-/-}$) and heterozygous (KChIP2$^{+/-}$) animals probed with the 5′ and 3′ probes; the WT (5′: 11.7 kb; 3′: 11.2 kb) and targeted (5′: 13.9 kb; 3′: 6.3 kb) alleles are indicated by arrows. *D*, Western blots of brain lysates probed with a mouse monoclonal anti-KChIP2 antibody confirmed that no KChIP2 protein (arrow) is detected in KChIP2$^{-/-}$ animals.

constant (τ_{rec}) of 51 ± 5 ms ($n = 8$), is also undetectable in KChIP2$^{-/-}$ LVA myocytes (Fig. 2*D*), consistent with the complete loss of $I_{to,f}$. In addition, although $I_{to,f}$ is expressed in the majority (~80%) of WT septum cells (Xu *et al.* 1999*b*; Brunet *et al.* 2004; Guo *et al.* 2005), $I_{to,f}$ is also undetectable (Fig. 2*A*) in all KChIP2$^{-/-}$ septum cells (Table 2).

As described previously (Guo *et al.* 1999, 2005; Xu *et al.* 1999*b*; Brunet *et al.* 2004), the decay phases of the Kv currents recorded from WT LVA cells at room temperature are best described by the sum of two exponentials with decay time constants (τ_{decay}) of 78 ± 5 ms and 1210 ± 43 ms ($n = 37$), reflecting $I_{to,f}$ and $I_{K,slow}$ (Fig. 2*B*). Although the rapidly inactivating current component is not evident in recordings from KChIP2$^{-/-}$ LVA myocytes (Fig. 2*A*), two components were also required to fit the decay phases of the outward currents in these cells (Fig. 2*B*); the τ_{decay} values for these components were

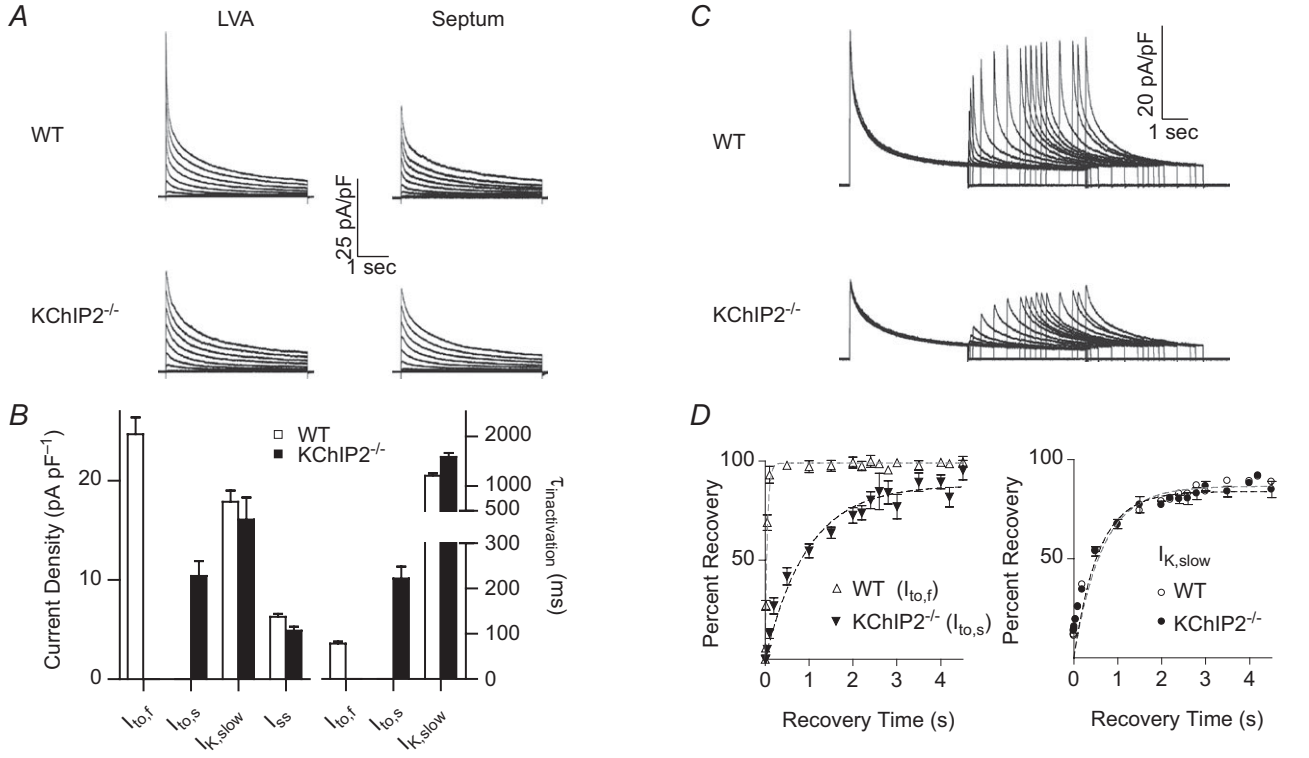

Figure 2. The rapidly inactivating and recovering $I_{to,f}$ is eliminated and electrical remodelling is evident in KChIP2$^{-/-}$ ventricular myocytes

A, representative whole-cell Kv currents, recorded at room temperature from WT and KChIP2$^{-/-}$ left ventricular apex (LVA) and interventricular septum (septum) myocytes in response to 4.5 s depolarizing voltage steps to test potentials between −60 and +40 mV (10 mV increments) from a holding potential of −70 mV; recorded currents were normalized for differences in cell size (whole-cell membrane capacitance) and current densities are plotted. As is evident, the rapid component of current decay, which is prominent in WT LVA cells, is absent in KChIP2$^{-/-}$ LVA myocytes, and the waveforms of the currents in the KChIP2$^{-/-}$ LVA and septum cells are quite similar. The decay phases of the outward Kv currents in WT and KChIP2$^{-/-}$ LVA cells were fitted to the sum of two exponentials and the mean current densities and $I_{to,f}$ ($I_{to,s}$) and $I_{K,slow}$ inactivation time constants, determined from these fits, in WT ($n = 37$) and KChIP2$^{-/-}$ ($n = 12$) LVA myocytes, are presented in *B*. Similar analyses were completed to determine the amplitudes/densities and inactivation kinetics of the Kv currents in septum cells (see text). To examine the kinetics of Kv current recovery from inactivation, a three-pulse protocol was used: after inactivating the currents during 4.5 s pre-pulses to +30 mV, LVA cells were hyperpolarized to −70 mV for varying times (5 ms to 4.5 s) before test depolarizations to +30 mV (*C*). Representative current waveforms, recorded using this protocol from WT and KChIP2$^{-/-}$ LVA cells, are illustrated. As is evident, no rapidly recovering current is present in KChIP2$^{-/-}$ LVA cells. The amplitudes of $I_{to,f}$ and $I_{K,slow}$ in WT LVA cells and the amplitudes of $I_{to,s}$ and $I_{K,slow}$ in KChIP2$^{-/-}$ LVA cells (at +30 mV) after each recovery period were determined from double exponential fits to the decay phases of the currents (see Methods). These values were normalized to the current amplitudes in the same cell evoked after the 10 s recovery period and mean normalized recovery data for $I_{to,f}$ (△) in WT LVA cells and $I_{to,s}$ (▼), in KChIP2$^{-/-}$ LVA cells and for $I_{K,slow}$ (○,●) in WT ($n = 8$) and KChIP2$^{-/-}$ ($n = 11$) LVA cells are plotted as a function of recovery time in *D*; the recovery data for each of the currents are well described by single exponentials (dotted lines). The time constants (τ_{rec}) for $I_{to,f}$ and $I_{to,s}$ recovery determined from these fits in WT and KChIP2$^{-/-}$ LVA myocytes are 51 ± 1 and 1213 ± 285 ms, respectively. The τ_{rec} determined for $I_{K,slow}$ in KChIP2$^{-/-}$ (385 ± 17 ms) and WT (415 ± 21 ms) LVA myocytes are not significantly different.

Table 2. Kv current densities in adult WT and KChIP2$^{-/-}$ ventricular myocytes

	n	I_{peak} (pA pF^{-1})	$I_{to,f}$ (pA pF^{-1})	$I_{to,s}$ (pA pF^{-1})	$I_{K,slow}$ (pA pF^{-1})	I_{ss} (pA pF^{-1})
Wild type						
LV apex	37	50.2 ± 2.8	24.7 ± 1.7	ND	17.9 ± 1.1	6.3 ± 0.3
Septum with $I_{to,f}$	13	40.2 ± 4.9	11.0 ± 1.9	10.9 ± 2.6	13.9 ± 2.3	5.3 ± 0.4
Septum without $I_{to,f}$	7	30.7 ± 4.3	ND	7.8 ± 1.5	16.4 ± 2.0	5.5 ± 0.5
KChIP2$^{-/-}$						
LV apex	12	32.3 ± 4.0$^{\#}$	ND	10.4 ± 1.5	16.1 ± 2.2	4.9 ± 0.4
Septum with $I_{to,f}$	0	—	—	—	—	—
Septum without $I_{to,f}$	8	26.0 ± 1.9	ND	6.4 ± 0.7	14.1 ± 1.0	5.5 ± 0.3

Current densities were determined from analyses of currents recorded at room temperature in response to 4.5 s depolarizations to +40 mV from a holding potential of −70 mV. All values are means ± SEM; n = numbers of cells studied; ND = not detected. $^{\#}$Peak current density is significantly ($P < 0.01$) lower in KChIP2$^{-/-}$, compared with WT, LVA myocytes.

223 ± 26 and 1586 ± 79 ms ($n = 12$). The time constant (1586 ± 79 ms) for the slower component of current decay in KChIP2$^{-/-}$ LVA myocytes is similar to the τ_{decay} determined for $I_{K,slow}$ in WT LVA cells (1210 ± 43 ms) and the mean densities of this ($I_{K,slow}$) current component in KChIP2$^{-/-}$ and WT LVA cells are not significantly different (Fig. 2*B*; Table 2). In WT LVA cells, $I_{K,slow}$ also recovers from inactivation much more slowly than $I_{to,f}$ (Fig. 2*C* and *D*). The time constant of $I_{K,slow}$ recovery in KChIP2$^{-/-}$ ($n = 11$) LVA myocytes was 385 ± 17 ms, a value that is not significantly different from the τ_{rec} (415 ± 21 ms) of $I_{K,slow}$ in WT ($n = 8$) LVA cells (Fig. 2*D*). Similar analyses revealed that $I_{K,slow}$ densities and properties in WT and KChIP2$^{-/-}$ septum cells are also not significantly different (Table 2).

The time constant of inactivation of the faster component of outward current decay (223 ± 26 ms) in KChIP2$^{-/-}$ LVA myocytes is similar to the τ_{decay} for $I_{to,s}$ in WT septum cells, suggesting that $I_{to,s}$ is upregulated in parallel with the loss of $I_{to,f}$ in KChIP2$^{-/-}$ LVA myocytes. Further experiments revealed that the time constant of recovery of this component of current decay in KChIP2$^{-/-}$ LVA myocytes was 1213 ± 285 ms, which is also similar to the previously reported τ_{rec} (1298 ms) for $I_{to,s}$ in WT septum cells (Xu *et al.* 1999*b*). Taken together, these results suggest that the rapidly inactivating, slowly recovering current in KChIP2$^{-/-}$ LVA myocytes reflects the upregulation of $I_{to,s}$, results similar to those reported previously in myocytes isolated from Kv4.2$^{-/-}$ and Kv4.2DN mice (Barry *et al.* 1998; Guo *et al.* 2005). The conclusion that $I_{to,s}$ is ugregulated in KChIP2$^{-/-}$ LVA cells, however, is quite different from the conclusion of Thomsen *et al.* (2009*a*), who reported that the Kv1.5-encoded component of $I_{K,slow}$, $I_{K,slow1}$ (London *et al.* 1998, 2001; Li *et al.* 2004) is increased in ventricular myocytes isolated from the *KChIP2*$^{-/-}$ mice generated by Kuo *et al.* (2001).

Although the analyses of the currents evoked during 4.5 s depolarizations at room temperature (Fig. 2) revealed no significant differences in (total) $I_{K,slow}$ in KChIP2$^{-/-}$ and WT LVA (or septum) myocytes, these experiments do not permit the resolution of the two components of $I_{K,slow}$, $I_{K,slow1}$ and $I_{K,slow2}$ (Xu *et al.* 1999*a*; Brunet *et al.* 2004; Liu *et al.* 2011). Additional experiments were therefore conducted in which Kv current waveforms, evoked during prolonged (20 s) depolarizations, were recorded and analysed. Consistent with the findings of Liu *et al.* (2011), the waveforms of the Kv currents evoked in WT mouse ventricular myocytes during 20 s depolarizing voltage steps at room temperature (Fig. 3*A*) were well described by the sum of three exponentials (Fig. 3*B*), corresponding to $I_{to,f}$, $I_{K,slow1}$ and $I_{K,slow2}$. Analyses of the Kv currents recorded from KChIP2$^{-/-}$ cells using the same voltage-clamp paradigm (Fig. 3*A*) also revealed that the decay phases of the currents were well described by the sum of three exponentials (Fig. 3*B*). The decay time constant of the rapidly decaying Kv current component in these KChIP2$^{-/-}$ cells is slower than in WT cells, reflecting the upregulation of $I_{to,s}$. The time constants and the densities of the two slower components of current decay, $I_{K,slow1}$ and $I_{K,slow2}$, determined from these fits in WT and KChIP2$^{-/-}$ LVA cells are indistinguishable (Fig. 3*C*; Table 3). In contrast to the conclusions of Thomsen and colleagues, we therefore find no evidence for upregulation of $I_{K,slow1}$ in ventricular myocytes from animals lacking KChIP2 and $I_{to,f}$ (see Discussion). Rather, the loss of KChIP2 and $I_{to,f}$ is accompanied by the upregulation of $I_{to,s}$, a current not present in WT LVA myocytes (Xu *et al.* 1999*a*; Brunet *et al.* 2004; Guo *et al.* 2005; Liu *et al.* 2011).

ECG waveforms are unaffected by the loss of KChIP2

As is evident in the representative ECG recordings in Fig. 4*A*, the heart rates and the morphologies of the P waves, QRS complexes and T waves in adult (8–15 weeks) WT and KChIP2$^{-/-}$ animals are indistinguishable. Statistical analysis revealed no significant differences in the durations of the RR, PR, QRS or QT intervals in WT ($n = 8$) and

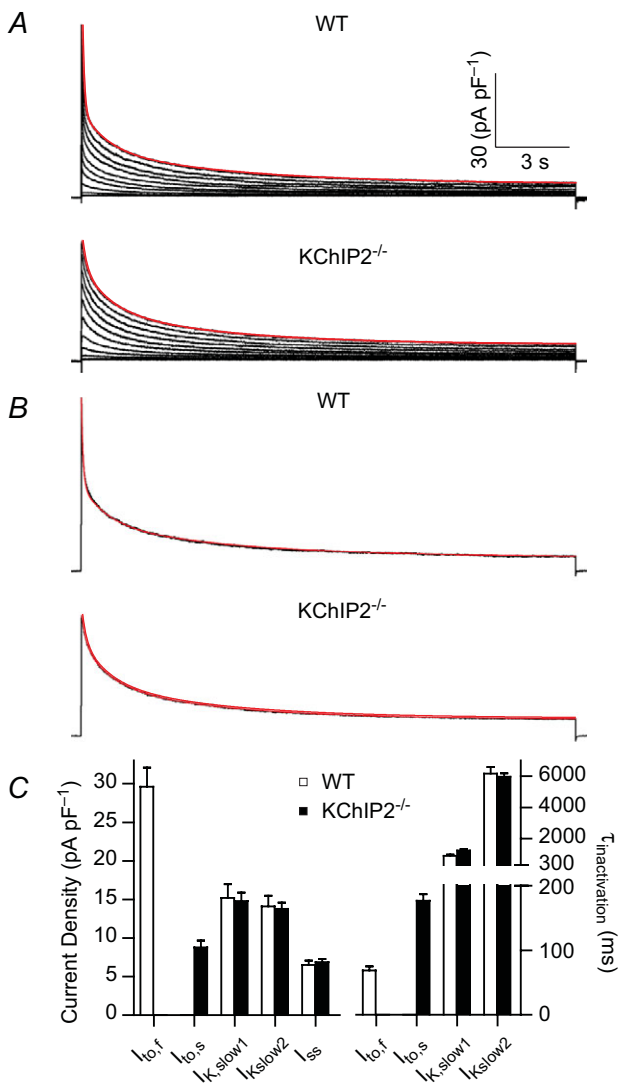

Figure 3. Neither component of $I_{K,slow}$, $I_{K,slow1}$ or $I_{K,slow2}$, is measurably altered in KChIP2$^{-/-}$ ventricular myocytes
A, representative whole-cell Kv currents, recorded at room temperature from WT and KChIP2$^{-/-}$ LVA myocytes in response to 20 s depolarizing voltage steps to test potentials between −60 and +60 mV (in 10 mV increments) from a holding potential of −70 mV; the currents were normalized to the whole cell membrane capacitance (in the same cell) and current densities are plotted. Outward currents (from the two representative cells in *A*) evoked at +60 mV are replotted in *B* and three-exponential fits to the decay phases of the currents are plotted as lines (in red) superimposed on the experimental data plotted as points (in black). The mean densities of $I_{to,f}$ ($I_{to,s}$), $I_{K,slow1}$, $I_{K,slow2}$ and I_{ss}, and the mean time constants of $I_{to,f}$ ($I_{to,s}$), $I_{K,slow1}$ and $I_{K,slow2}$ inactivation, determined from these fits, in WT ($n = 8$) and KChIP2$^{-/-}$ ($n = 19$) LVA myocytes are presented in *C*. As is evident, the densities and the time constants of inactivation of $I_{K,slow1}$ and $I_{K,slow2}$ in WT and KChIP2$^{-/-}$ LVA myocytes are not significantly different (see text).

KChIP2$^{-/-}$ ($n = 7$) animals (Fig. 4*B*); mean corrected QT (QT_c) intervals determined in KChIP2$^{-/-}$ ($n = 8$) and WT ($n = 7$) animals were not significantly different.

The finding that ECG recordings from KChIP2$^{-/-}$ and WT animals are indistinguishable was surprising given the loss of $I_{to,f}$ and the marked alterations in peak Kv current densities measured in isolated KChIP2$^{-/-}$ compared with WT LVA myocytes (Fig. 2). In addition, it was previously reported that the targeted deletion of KChIP2 results in action potential prolongation in KChIP2$^{-/-}$ ventricular myocytes (Kuo *et al.* 2001). As illustrated in Fig. 5, however, action potentials recorded from KChIP2$^{-/-}$ ($n = 14$) and WT ($n = 13$) LVA myocytes at physiological temperatures (35–37°C) are similar (Fig. 5*A*). Indeed, there are no significant differences in APD_{20}, APD_{50} and APD_{90} (Fig. 5*B*) values in WT and KChIP2$^{-/-}$ LVA myocytes at physiological temperature.

The observation that action potential waveforms recorded in WT and KChIP2$^{-/-}$ LVA myocytes at physiological temperatures are similar (Fig. 5*A* and *B*) is consistent with the ECG findings (Fig. 4). These observations, however, appear to be inconsistent with the voltage-clamp data (Fig. 2; Table 2) obtained at room temperature, suggesting that the repolarizing Kv currents in KChIP2$^{-/-}$ and WT LVA myocytes are differently affected by temperature. Whole-cell voltage-clamp experiments, designed to explore this hypothesis directly, indeed revealed that outward Kv current waveforms recorded from WT and KChIP2$^{-/-}$ LVA myocytes at physiological temperature are quite similar (Fig. 5*C*). Analyses of the Kv current waveforms revealed that, although peak Kv current densities determined at room temperature in KChIP2$^{-/-}$ LVA cells are significantly lower than in WT LVA cells (Fig. 5*D*), the difference is less than at room temperature, an observation that appears to reflect the relatively higher density of $I_{to,s}$ in KChIP2$^{-/-}$ LVA cells at physiological (Fig. 5*D*) than at room (Fig. 2*C*) temperature. Analyses of the Kv current records obtained at physiological temperature revealed that the decay phase of the currents in WT and KChIP2$^{-/-}$ LVA myocytes are best described by the sum of three exponentials, corresponding to $I_{to,f}$, $I_{K,slow1}$ and $I_{K,slow2}$ in WT cells and to $I_{to,s}$, $I_{K,slow1}$ and $I_{K,slow2}$ in KChIP2$^{-/-}$ cells (Fig. 5; Table 3). These analyses confirmed that $I_{K,slow1}$, and $I_{K,slow2}$ densities and kinetics in WT and KChIP2$^{-/-}$ LVA myocytes are not significantly different (Fig. 5*D*; Table 3). Interestingly, I_{ss} densities in both WT and KChIP2$^{-/-}$ LVA myocytes are significantly higher (~2-fold) in recordings obtained at physiological than at room temperature.

Further experiments revealed that, in contrast to the results obtained at physiological temperature (Fig. 5*A*; Fig. 5*B*), but consistent with the previously reported results of Kuo *et al.* (2001), evoked action potential durations recorded at room temperatures are significantly longer in KChIP2$^{-/-}$ ($n = 14$) than in WT ($n = 14$) LVA

Table 3. Comparisons of Kv current densities in adult WT and KChIP2$^{-/-}$ LVA myocytes determined from analyses of currents evoked during 20 s depolarizations at room temperature (22–23°C) or 4.5 s depolarizations at physiological temperature (35–37°C)

		I_{peak}	$I_{to,f}$		$I_{to,s}$		$I_{K,slow1}$		$I_{K,slow2}$		I_{ss}
	n	Density (pA pF^{-1})	Density (pA pF^{-1})	τ_{decay} (ms)	Density (pA pF^{-1})	τ_{decay} (ms)	Density (pA pF^{-1})	τ_{decay} (ms)	Density (pA pF^{-1})	τ_{decay} (ms)	Density (pA pF^{-1})
Room temperature (22–23°C)											
WT	10	56.5 ± 5.2	24.8 ± 4.1	67 ± 2	ND	ND	15.9 ± 4.6	878 ± 67	11.4 ± 0.9	5554 ± 179	4.5 ± 0.4
KChIP2$^{-/-}$	17	32.4 ± 1.8$^{\#}$	ND	ND	7.0 ± 0.9	220 ± 14	11.1 ± 0.7	1226 ± 48	9.7 ± 0.5	6092 ± 258	4.6 ± 0.2
Physiological temperature (35–37°C)											
WT	14	58.0 ± 3.4	19.1 ± 2.1	12 ± 3	ND	ND	16.4 ± 1.8	156 ± 19	13.6 ± 0.9	970 ± 83	8.7 ± 0.6
KChIP2$^{-/-}$	11	45.0 ± 3.3*	ND	ND	10.4 ± 1.0	38 ± 1.4	15.1 ± 1.2	236 ± 20	11.2 ± 1.1	1304 ± 142	8.5 ± 0.8

Current densities were determined from analyses of currents recorded during 20 s depolarizations to +40 mV from a holding potential of −70 mV at room (22–23°C) temperature or during 4.5 s depolarizations to +40 mV at physiological (35–37°C) temperature. All values are means ± SEM; n = numbers of cells studied; ND = not detected. Peak Kv current densities are significantly ($^{*}P < 0.05$, $^{\#}P < 0.01$) lower in KChIP2$^{-/-}$, compared with WT, LVA myocytes.

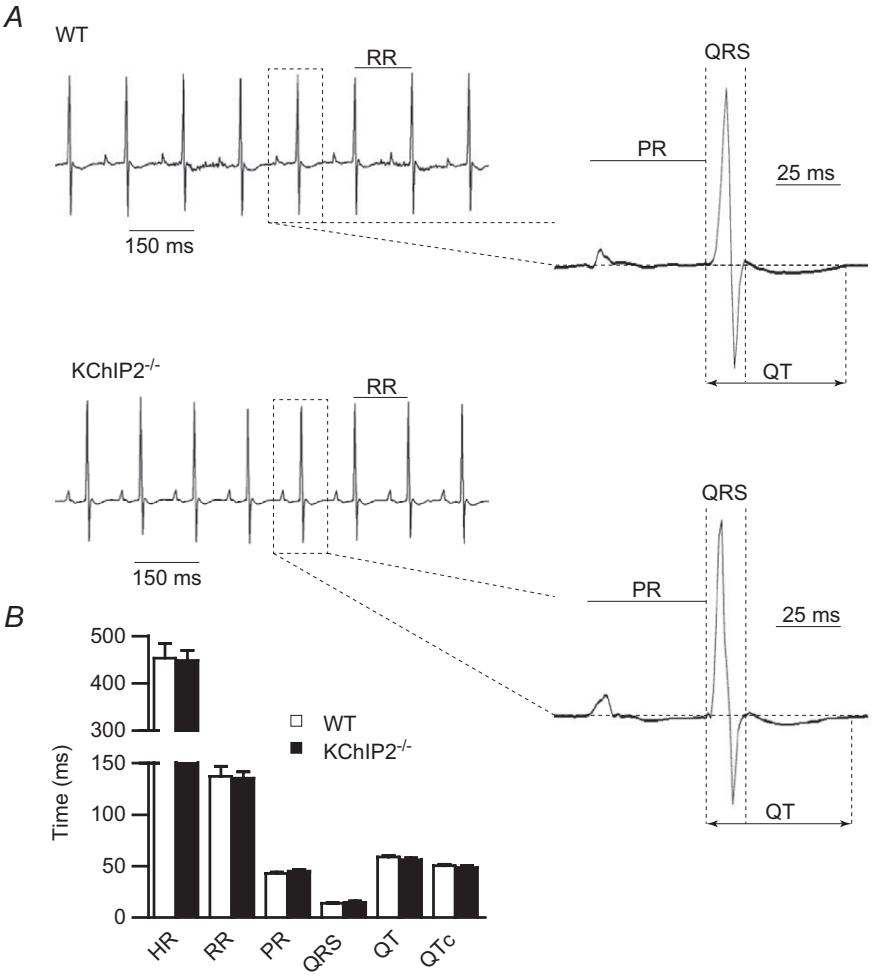

Figure 4. ECG waveforms are unaffected by the loss of KChIP2
A, representative telemetric ECG traces recorded from WT ($n = 8$) and KChIP2$^{-/-}$ ($n = 7$) animals are similar; no differences in heart rates or in the morphologies of the P waves, QRS complexes or T waves are evident. *B*, statistical analyses revealed no significant differences in the mean durations of the RR intervals, PR intervals, QRS complexes and QT intervals in WT and KChIP2$^{-/-}$ animals.

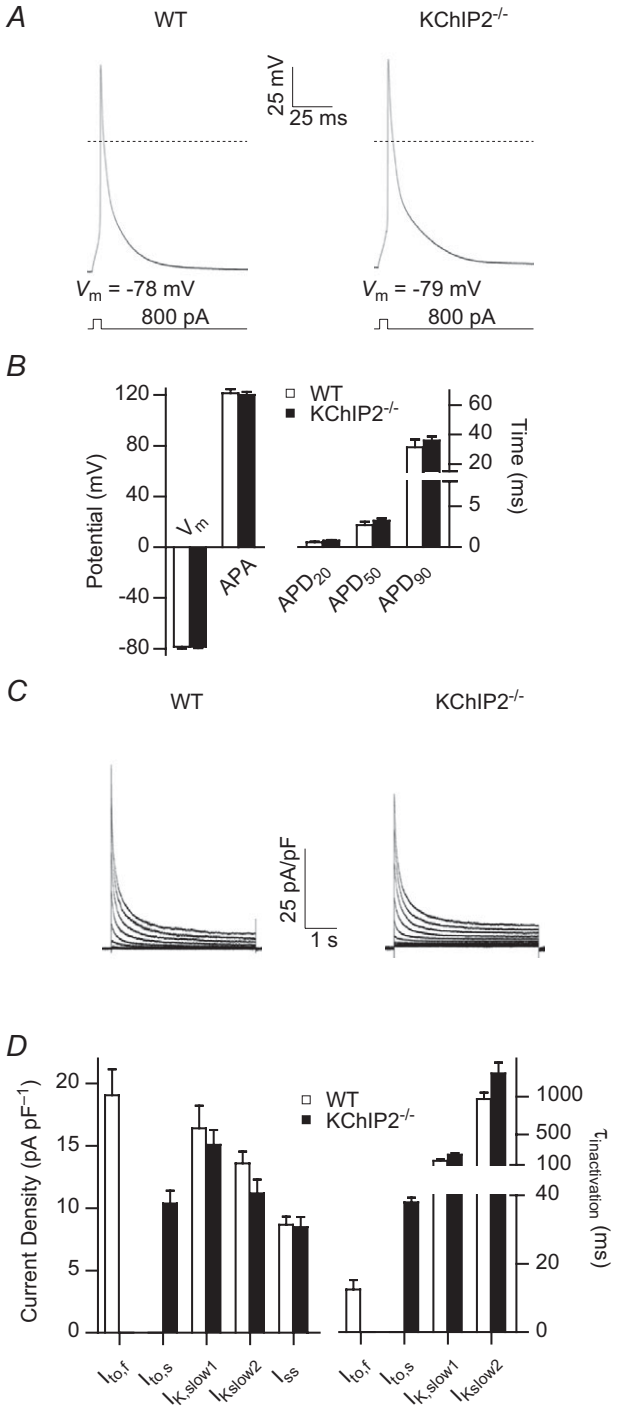

Figure 5. Action potential and Kv current waveforms recorded at physiological temperatures are similar in KChIP2$^{-/-}$ and WT LVA myocytes

A, representative action potentials, evoked in response to brief depolarizing current injections, in WT and KChIP2$^{-/-}$ LVA myocytes at 35–37°C are similar. *B*, mean resting membrane potentials (V_m), action potential amplitudes (APA) and action potential durations at 20% (APD_{20}), 50% (APD_{50}) and 90% (APD_{90}) repolarization are not significantly different in WT ($n = 13$) and KChIP2$^{-/-}$ ($n = 14$) LVA myocytes. *C*, representative whole-cell Kv currents, recorded at physiological temperature (35–37°C), from WT and KChIP2$^{-/-}$ LVA myocytes in response to 4.5 s depolarizing voltage steps to test potentials between −60 and +40 mV (in 10 mV increments) from a holding potential of −70 mV; recorded currents were normalized to the whole-cell membrane capacitance (in the same cell) and current densities are plotted. The decay phases of the currents were fitted to the sum of three exponentials to provide the amplitudes and the time constants of inactivation of the individual current components. *D*, mean densities of $I_{to,f}$ ($I_{to,s}$), $I_{K,slow1}$, $I_{K,slow2}$ and I_{ss}, as well as the mean time constants of $I_{to,f}$ ($I_{to,s}$), $I_{K,slow1}$ and $I_{K,slow2}$ inactivation, derived from these fits in WT ($n = 14$) and KChIP2$^{-/-}$ ($n = 11$) LVA myocytes.

myocytes (Fig. 6*A*). Action potential durations at 20% (APD_{20}, $P < 0.01$), 50% (APD_{50}, $P < 0.05$) and 90% (APD_{90}, $P < 0.05$) repolarization were 2.1 ± 0.2, 7.0 ± 1.0 and 56.6 ± 8.6 ms, respectively, in KChIP2$^{-/-}$ LVA myocytes (Fig. 6*B*), compared with 1.3 ± 0.1, 3.9 ± 0.4 and 28.7 ± 5.4 ms in WT LVA cells. These combined experiments illustrate the importance of conducting current- and voltage-clamp experiments at physiological temperatures to compare directly with ECG recordings (see Discussion).

Kv4.2 protein is undetectable in KChIP2$^{-/-}$ ventricles

As discussed in the Introduction, recent biochemical studies revealed that the binding of KChIP2 to Kv4.2 markedly increases total Kv4.2 protein (Foeger *et al.*), suggesting that the *in vivo* elimination of KChIP2 might lead to the destabilization and loss of the Kv4.2 protein, and that this underlies the observation that $I_{to,f}$ is undetectable in KChIP2$^{-/-}$ ventricular myocytes. Consistent with this hypothesis, Western blot analysis revealed that the Kv4.2 protein is undetectable in KChIP2$^{-/-}$ ventricles (Fig. 7*A*). In contrast, quantitative RT-PCR analysis revealed no difference (Fig. 7*C*) or small increases (Fig. 7*D* and *E*) in *Kcnd2* transcript levels in KChIP2$^{-/-}$, compared with WT, right and left ventricles and interventricular septa. The expression levels of transcripts encoding a number of other Kv channel α subunits were also examined in adult (8–14 weeks) WT ($n = 6$) and KChIP2$^{-/-}$ ($n = 6$) ventricular samples. These experiments revealed no significant differences in the expression levels of the *Kcna4* (Kv1.4), *Ncs1* (NCS-1), *Kcna5* (Kv1.5), *Kcnb1* (Kv2.1), *Kcnk2* (TREK1) or *Kcnk3* (TASK1) transcripts in KChIP2$^{-/-}$, compared with WT, left ventricles (Fig. 7*C*). In right ventricles (Fig. 7*D*), there was a small but statistically significant ($P < 0.05$) difference (decrease) in *Kcnd3* ($14 \pm 3\%$) expression. In the interventricular septum samples (Fig. 7*E*), *Kcnb1* ($13 \pm 5\%$) transcript was lower ($P < 0.05$) in samples from KChIP2$^{-/-}$, compared with WT, animals. In spite of the elimination of the Kv4.2 protein and the observed increase in $I_{to,s}$, therefore, there is very little evidence for transcriptional remodelling of the Kv4 or Kv1.4 subunits in KChIP2$^{-/-}$ ventricles. In

addition, in contrast to previously published findings (Thomsen *et al.* 2009*a*) using the *KChIP2*$^{-/-}$ model (Kuo *et al.* 2001), the targeted deletion of KChIP2 here did not measurably affect the expression of the *Kcna5* (Kv1.5) transcript.

Reintroduction of KChIP2 increases L-type Ca^{2+} currents, but does not rescue $I_{to,f}$, in KChIP2$^{-/-}$ myocytes

The observation that the *Kcnd2* transcript is unaffected in KChIP2$^{-/-}$ ventricles suggested the possibility that reintroduction of KChIP2 might rescue $I_{to,f}$. To test this hypothesis directly, KChIP2$^{-/-}$ myocytes were infected with an adenovirus encoding either tdTomato alone or tdTomato plus KChIP2. In contrast to our expectations, however, whole-cell Kv current waveforms recorded from tdTomato-expressing cells 36–48 h after viral infections in the absence and in the presence of KChIP2 were indistinguishable (Fig. 8*A*). There were no significant differences in the densities or properties of the Kv currents in KChIP2$^{-/-}$ myocytes expressing tdTomato alone or with KChIP2 (Fig. 8*B*). Kinetic analyses of the currents revealed that the decay phases of the currents in KChIP2$^{-/-}$ myocytes expressing tdTomato alone ($n = 7$) and tdTomato plus KChIP2 ($n = 4$) were best described by the sum of two exponentials and that the amplitudes/densities (Fig. 8*B*) and the time constants of decay of the currents ($I_{to,s}$, $I_{K,slow}$ and I_{ss}), determined from these fits, are not significantly different. The τ_{decay} values for the rapid component of decay in KChIP2$^{-/-}$ myocytes expressing tdTomato alone ($n = 7$) and tdTomato plus KChIP2 ($n = 4$), for example, were 258 ± 14 and 271 ± 21 ms, respectively, consistent with the expression of $I_{to,s}$.

It has previously been reported that L-type Ca^{2+} currents ($I_{Ca,L}$) are reduced in KChIP2$^{-/-}$ myocytes in spite of increased expression of the Cav1.2 protein, the α subunit which underlies $I_{Ca,L}$ (Thomsen *et al.* 2009*b*). In contrast to the results obtained for the Kv currents, however, reintroduction of KChIP2 in KChIP2$^{-/-}$ myocytes significantly ($P < 0.01$) increased Ca^{2+} current amplitudes/densities compared with KChIP2$^{-/-}$ cells expressing tdTomato alone (Fig. 8*D*; see Discussion).

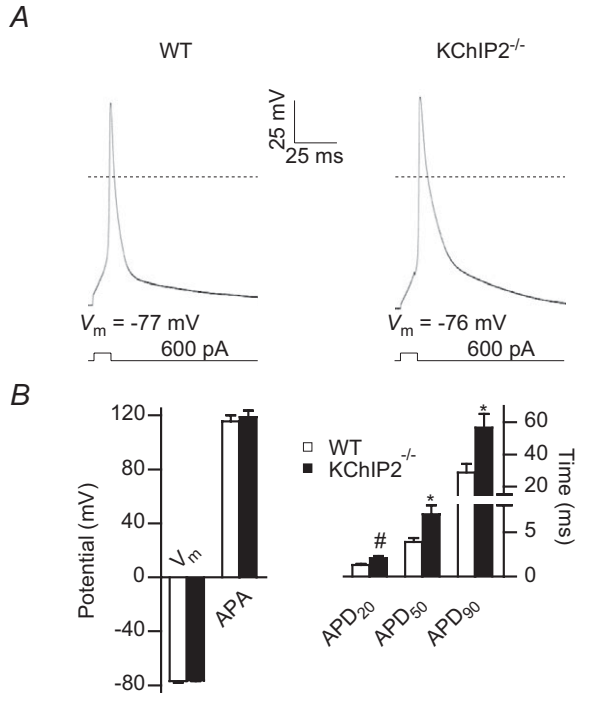

Figure 6. Action potentials recorded at room temperatures are prolonged in KChIP2$^{-/-}$, compared with WT, ventricular myocytes
A, representative action potentials, recorded at room temperature (22–23°C), in WT and KChIP2$^{-/-}$ LVA myocytes in response to brief depolarizing current injections. *B*, mean V_m and APA measured in KChIP2$^{-/-}$ ($n = 14$) and WT ($n = 14$) LVA cells at room temperature are not significantly different. In contrast to recordings obtained at physiological temperature (Fig. 5), however, mean APD_{20} ($^{\#}P < 0.01$), APD_{50} ($^{*}P < 0.05$) and APD_{90} ($^{*}P < 0.05$) values are significantly longer in recordings from KChIP2$^{-/-}$, compared with WT, LVA myocytes at room temperature.

Discussion

Targeted disruption of KChIP2 eliminates mouse ventricular $I_{to,f}$

Similar to the previous studies on the *KChIP2*$^{-/-}$ targeted deletion mice generated by Kuo *et al.* (2001) and later studied by Thomsen *et al.* (2009*a*), the results of the experiments here demonstrate that $I_{to,f}$ is eliminated in KChIP2$^{-/-}$ mouse ventricular myocytes. The experiments here also revealed that ECG waveforms in WT and KChIP2$^{-/-}$ mice are indistinguishable and that action potential waveforms recorded in WT and KChIP2$^{-/-}$ LVA myocytes are not measurably different at physiological temperature. Although these results are in apparent conflict with the report that action potentials are prolonged in ventricular myocytes isolated from the previously described *KChIP2*$^{-/-}$ model (Kuo *et al.* 2001), these earlier experiments were conducted at room temperature, not at physiological temperature. Indeed, additional experiments here confirmed that action potentials in KChIP2$^{-/-}$ ventricular myocytes are prolonged compared with action potentials in WT cells when recordings are obtained at room temperature. Also in contrast to the results here, ST segment elevation was reported in the *KChIP2*$^{-/-}$ mice by Kuo *et al.* (2001). These observations could reflect differences in the genetic background of the KChIP2$^{-/-}$ mice generated and studied in the present, compared with the previous (Kuo *et al.* 2001), study. Interestingly,

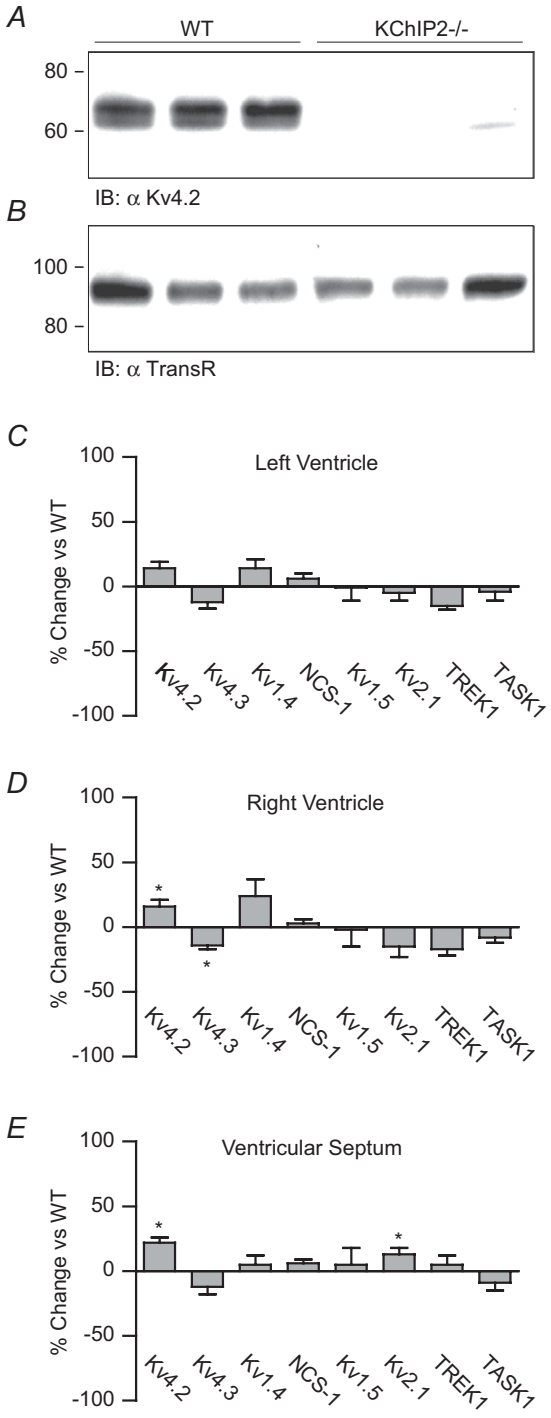

Figure 7. Kv4.2 protein is undetectable in KChIP2$^{-/-}$ ventricles
A, Western blots of membrane proteins prepared from WT and KChIP2$^{-/-}$ ventricles, probed with a rabbit polyclonal anti-Kv4.2 antibody, revealed that the Kv4.2 protein is undetectable in KChIP2$^{-/-}$ ventricles. The blots were also probed with a mouse monoclonal anti-transferrin receptor antibody to ensure equal protein loading of the samples (*B*). The expression levels of the transcripts encoding multiple Kv channel subunits in adult (8–14 weeks) WT ($n = 6$) and KChIP2$^{-/-}$ ($n = 6$) left ventricles (*C*), right ventricles (*D*) and interventricular septa (*E*) were examined using SYBR green quantitative RT-PCR. Mean percentage changes in the relative expression levels of each transcript in KChIP2$^{-/-}$, compared with WT, left ventricles (*C*), right ventricles (*D*) and septa (*E*) are plotted. As is evident, in contrast to the Kv4.2 protein, the *Kcnd2* transcript is not eliminated in KChIP2$^{-/-}$ ventricles. Indeed, the *Kcnd2* transcript was modestly, but significantly ($^*P < 0.05$), increased in the KChIP2$^{-/-}$ right ventricular and interventricular septum samples. The expression levels of the transcripts encoding the other Kvα subunits in KChIP2$^{-/-}$ ventricles were also similar to WT levels. There was a modest (~10%) increase in the *Kcnb1* ($^*P < 0.05$) transcript in KChIP2$^{-/-}$ interventricular septa and the *Kcnd3* transcript was modestly ($^*P < 0.05$) decreased in KChIP2$^{-/-}$ right ventricles.

however, ST segment elevation is not evident in the ECG recordings from the *KChIP2*$^{-/-}$ mice reported by Thomsen and colleagues (2009b), suggesting that some other experimental variable(s) underlies the phenotype previously reported by Kuo and colleagues (2001).

Voltage-clamp experiments conducted here at room temperature revealed that peak Kv current densities are significantly lower in KChIP2$^{-/-}$ than in WT LVA myocytes. This result differs from the findings of Thomsen *et al.* (2009*a*). In the previous study, however, depolarizing prepulses to −20 mV for 25 ms (presented to inactivate voltage-dependent Na^+ currents) were applied prior to the test depolarizations to evoke $I_{to,f}$ (Thomsen *et al.* 2009*a*). The use of this prepulse, however, would be expected to partially inactivate $I_{to,f}$. Indeed, Thomsen *et al.* (2009*a*) reported peak whole-cell Kv current densities at +40 mV in WT LV myocytes of ~30 pA pF^{-1}, a value that is much lower than the peak Kv current densities in WT LVA myocytes reported here (Tables 2 and 3) and in numerous previous studies (Guo *et al.* 1999; Xu *et al.* 1999*b*; Brunet *et al.* 2004).

In KChIP2$^{-/-}$ ventricles, the Kv4.2 protein is undetectable, although this finding does not reflect transcriptional remodelling as *Kcnd2* (Kv4.2) transcript levels are not decreased in KChIP2$^{-/-}$, compared with WT, ventricles (Fig. 7). Interestingly, these results mirror observations in Kv4.2$^{-/-}$ animals (Guo *et al.* 2005), in which KChIP2 protein expression was reduced >90% in Kv4.2$^{-/-}$ ventricles, whereas expression of the *Kcnip2* transcript was similar in Kv4.2$^{-/-}$ and WT ventricles. Taken together with recent studies demonstrating that the association (binding) of KChIP2 and Kv4.2 results in the reciprocal stabilization of both (the Kv4.2 and KChIP2) proteins (Foeger *et al.* 2010), these results suggest that Kv4/KChIP complex formation is *required* for the generation of functional myocardial Kv4-encoded $I_{to,f}$ channels.

Loss of $I_{to,f}$ in KChIP2$^{-/-}$ ventricular myocytes is associated with Kv current remodelling

The results here demonstrate that the elimination of $I_{to,f}$ in KChIP2$^{-/-}$ ventricular myocytes is accompanied by

an increase in a slowly inactivating, slowly recovering Kv current with properties very similar to $I_{to,s}$ in WT interventricular septum myocytes (Xu *et al.* 1999*b*; Guo *et al.* 2000). These results are similar to previously reported findings in (Kv4.2$^{-/-}$) mice harbouring a targeted disruption of the *Kcnd2* (Kv4.2) locus (Guo *et al.* 2005), as well as in mice with cardiac-specific expression of a mutant Kv4.2 α subunit (Kv4.2DN) that functions as a dominant negative (Barry *et al.* 1998; Guo *et al.* 2000). In ventricular myocytes from both of these lines of mice, $I_{to,s}$ is upregulated in parallel with the elimination of Kv4.2-encoded $I_{to,f}$.

The findings here that there are two components of macroscopic current decay and that $I_{to,s}$ is increased in LVA myocytes in parallel with the loss of $I_{to,f}$ conflict with the findings of Kuo *et al.* (2001) and Thomsen *et al.* (2009*a*). In both of these previous reports, for example, it was stated that decay phases of the Kv current from *KChIP2*$^{-/-}$ ventricular myocytes at room temperature were well described by single exponentials. The durations of the depolarizing test pulses of 200 ms (Kuo *et al.* 2001) and 400 ms (Thomsen *et al.* 2009*a*) used in these studies, however, are too short to allow resolution of (the amplitudes or the τ_{decay} values of) $I_{to,s}$ and $I_{K,slow}$. Interestingly, in subsequent experiments conducted using longer (4.5 s) depolarizing voltage steps, Thomsen *et al.* (2009*a*) reported that whole-cell Kv currents in *KChIP2*$^{-/-}$ ventricular myocytes were well described by two components of inactivation with τ_{decay} values of ∼200 and ∼1250 ms, values that are very similar to those reported here.

Based on the finding of increased *Kcna5* (Kv1.5) expression and the results of pharmacological experiments with 4-aminopyridine (4-AP), it was previously suggested that the Kv1.5-encoded component of $I_{K,slow}$, $I_{K,slow1}$, was up-regulated in *KChIP2*$^{-/-}$ myocytes (Thomsen *et al.* 2009*a*). The analysis here, however, revealed no differences in $I_{K,slow1}$ in WT and KChIP2$^{-/-}$ myocytes. This apparent discrepancy may reflect the different (*KChIP2*$^{-/-}$ and KChIP2$^{-/-}$) mouse models used. Alternatively, it is possible that the (50 μM) concentrations of 4-AP used in the previous studies (Thomsen *et al.* 2009*a*) blocked

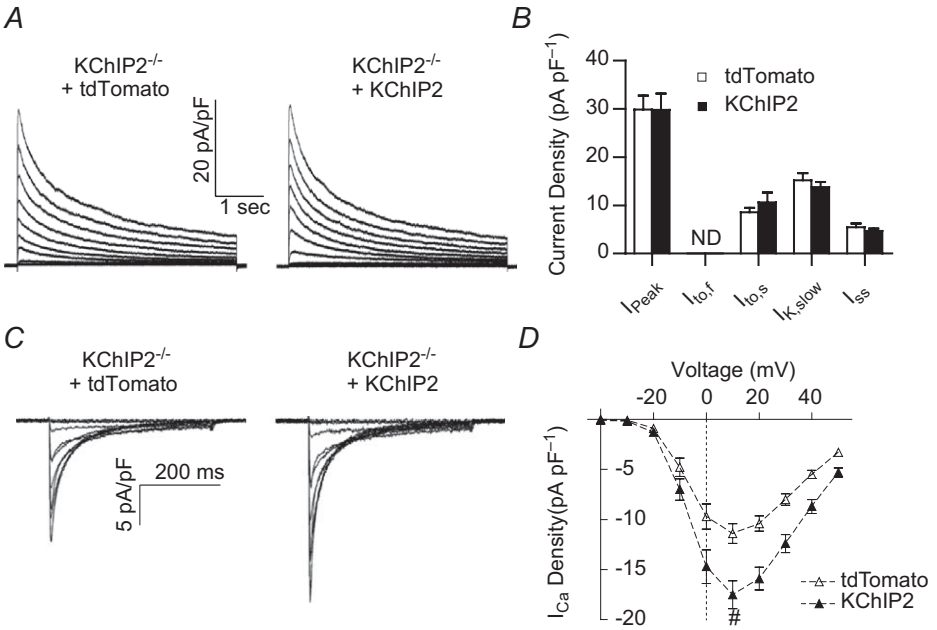

Figure 8. Increased expression of KChIP2 does not rescue $I_{to,f}$ in KChIP2$^{-/-}$ myocytes, but does augment L-type Ca^{2+} current densities
Isolated KChIP2$^{-/-}$ ventricular myocytes were infected with an adenoviral construct encoding either tdTomato alone or tdTomato with KChIP2 (see Methods). Whole-cell Kv currents were recorded 36–48 h later from tdTomato-expressing cells as described in the legend to Fig. 2; currents were normalized to the whole-cell membrane capacitance (in the same cell) and current densities are plotted. *A*, Kv current waveforms in KChIP2$^{-/-}$ cells expressing tdTomato alone and tdTomato with KChIP2 are indistinguishable. *B*, mean peak Kv current, $I_{to,s}$, $I_{K,slow}$ and I_{ss} densities in tdTomato- ($n = 7$) and tdTomato + KChIP2- ($n = 4$) expressing KChIP2$^{-/-}$ cells are not significantly different. *C*, whole-cell Cav currents, evoked in response to 400 ms depolarizing voltage steps to −40 to +50 mV (10 mV increments) from a holding potential of −70 mV, were also recorded from KChIP2$^{-/-}$ myocytes 36–48 h after infection with the tdTomato or tdTomato + KChIP2 adenovirus; recorded currents were normalized to whole-cell membrane capacitance (in the same cell), and current densities are plotted. *D*, mean Cav current densities are significantly ($^{\#}P < 0.01$) higher in tdTomato + KChIP2-expressing KChIP2$^{-/-}$ cells ($n = 13$) than in tdTomato-expressing KChIP2$^{-/-}$ cells ($n = 14$).

a portion of Kv1.4-encoded $I_{to,s}$, in addition to $I_{K,slow}$ (Stuhmer *et al.* 1989; Gutman *et al.* 2005), in *KChIP2*$^{-/-}$ ventricular myocytes.

KChIP2 regulates the functional expression of $I_{to,f}$ and $I_{Ca,L}$ by distinct mechanisms

Given the presence of the *Kcnd2* transcript in KChIP2$^{-/-}$ ventricles, it is perhaps surprising that reintroduction of KChIP2 fails to rescue $I_{to,f}$. While it is possible that an extremely slow turnover rate of $I_{to,f}$ channel complexes precluded detection of 'rescued' currents 36–48 h after KChIP2 expression, previous studies have suggested that the half-life of functional Kv4.2/KChIP2 channel complexes is ∼4 h, at least in heterologous cells (Shibata *et al.* 2003; Foeger *et al.* 2010). Given that KChIP proteins associate with nascent Kv4 α subunits early in the biosynthetic pathway (Hasdemir *et al.* 2005), it is also possible that a novel mechanism, such as compartmentalized translation of the (*Kcnd2* and *Kcnip2*) transcripts (Kislauskis *et al.* 1993; Besse & Ephrussi, 2008), plays a role in the assembly and processing of native cardiac $I_{to,f}$ channel complexes. If exogenously expressed *Kcnip2* message failed to properly co-localize with the endogenous *Kcnd2* transcript, functional Kv4.2–KChIP2 protein–protein interactions would not occur and $I_{to,f}$ channels would not be expressed.

Consistent with previous findings (Thomsen *et al.* 2009*b*), L-type Ca^{2+} currents ($I_{Ca,L}$) are reduced, but not eliminated, in KChIP2$^{-/-}$ ventricular myocytes. The results of Thomsen *et al.* (2009b) suggest that KChIP2 mediates augmentation of $I_{Ca,L}$ by binding to Cav1.2 and impeding the action of the N-terminal inhibitory domain of Cav1.2. In this model, the loss of the KChIP2 protein allows the N-terminal inhibitory domain to bind, and $I_{Ca,L}$ is decreased. Based on this model, it seemed reasonable to expect that the reintroduction of KChIP2 in the KChIP2$^{-/-}$ null background would 'rescue' the inhibition and increase $I_{Ca,L}$. The experiments here revealed that reintroduction of KChIP2 does indeed increase $I_{Ca,L}$ densities in KChIP2$^{-/-}$ ventricular myocytes. Interestingly, in marked contrast, expression of KChIP2 does *not* rescue $I_{to,f}$ in KChIP2$^{-/-}$ ventricular myocytes. In addition, in contrast to the loss of the Kv4.2 protein demonstrated here, Thomsen *et al.* (2009*b*) reported that expression of the Cav1.2 protein, the pore-forming subunit encoding mouse ventricular $I_{Ca,L}$, is similar in KChIP2$^{-/-}$ and WT ventricles. The molecular mechanism underlying KChIP2-mediated effects on Cav1.2-encoded $I_{Ca,L}$, therefore, are distinct from the stabilizing role of KChIP2–Kv4 protein–protein interactions critical for the generation of Kv4-encoded $I_{to,f}$ channels.

References

Aimond F, Kwak SP, Rhodes KJ & Nerbonne JM (2005). Accessory Kvβ_1 subunits differentially modulate the functional expression of voltage-gated K^+ channels in mouse ventricular myocytes. *Circ Res* **96**, 451–458.

An WF, Bowlby MR, Betty M, Cao J, Ling HP, Mendoza G, Hinson JW, Mattsson KI, Strassle BW, Trimmer JS & Rhodes KJ (2000). Modulation of A-type potassium channels by a family of calcium sensors. *Nature* **403**, 553–556.

Antzelevitch C, Sicouri S, Litovsky S, Lukas A, Krishnan S, Di Diego J, Gintant G & Liu D (1991). Heterogeneity within the ventricular wall. Electrophysiology and pharmacology of epicardial, endocardial, and M cells. *Circ Res* **69**, 1427–1449.

Bähring R, Dannenberg J, Peters HC, Leicher T, Pongs O & Isbrandt D (2001). Conserved Kv4 N-terminal domain critical for effects of Kv channel-interacting protein 2.2 on channel expression and gating. *J Biol Chem* **276**, 23888–23894.

Barry DM, Xu H, Schuessler RB & Nerbonne JM (1998). Functional knockout of the transient outward current, long-QT syndrome, and cardiac remodeling in mice expressing a dominant-negative Kv4 alpha subunit. *Circ Res* **83**, 560–567.

Besse F & Ephrussi A (2008). Translational control of localized mRNAs: restricting protein synthesis in space and time. *Nat Rev Mol Cell Biol* **9**, 971–980.

Brunet S, Aimond F, Li H, Guo W, Eldstrom J, Fedida D, Yamada KA & Nerbonne JM (2004). Heterogeneous expression of repolarizing, voltage-gated K^+ currents in adult mouse ventricles. *J Physiol* **559**, 103–120.

Dai S, Hall DD & Hell JW (2009). Supramolecular assemblies and localized regulation of voltage-gated ion channels. *Physiol Rev* **89**, 411–452.

Diwan A, Krenz M, Syed FM, Wansapura J, Ren X, Koesters AG, Li H, Kirshenbaum LA, Hahn HS, Robbins J, Jones WK & Ii GWD (2007). Inhibition of ischemic cardiomyocyte apoptosis through targeted ablation of Bnip3 restrains postinfarction remodeling in mice. *J Clin Invest* **117**, 2825–2833.

Diwan A, Matkovich SJ, Yuan Q, Zhao W, Yatani A, Brown JH, Molkentin JD, Kranias EG & Dorn GW (2009). Endoplasmic reticulum-mitochondria crosstalk in NIX-mediated murine cell death. *J Clin Invest* **119**, 203–212.

Foeger NC, Marionneau C & Nerbonne JM (2010). Co-assembly of Kv4 α subunits with K^+ channel-interacting protein 2 stabilizes protein expression and promotes surface retention of channel complexes. *J Biol Chem* **285**, 33413–33422.

Greenstein JL, Wu R, Po S, Tomaselli GF & Winslow RL (2000). Role of the calcium-independent transient outward current I_{to1} in shaping action potential morphology and duration. *Circ Res* **87**, 1026–1033.

Guo W, Jung WE, Marionneau C, Aimond F, Xu H, Yamada KA, Schwarz TL, Demolombe S & Nerbonne JM (2005). Targeted deletion of Kv4.2 eliminates $I_{to,f}$ and results in electrical and molecular remodeling, with no evidence of ventricular hypertrophy or myocardial dysfunction. *Circ Res* **97**, 1342–1350.

Guo W, Li H, Aimond F, Johns DC, Rhodes KJ, Trimmer JS & Nerbonne JM (2002). Role of heteromultimers in the generation of myocardial transient outward K^+ currents. *Circ Res* **90**, 586–593.

Guo W, Li H, London B & Nerbonne JM (2000). Functional consequences of elimination of $I_{to,f}$ and $I_{to,s}$: early afterdepolarizations, atrioventricular block, and ventricular arrhythmias in mice lacking Kv1.4 and expressing a dominant-negative Kv4 α subunit. *Circ Res* **87**, 73–79.

Guo W, Xu H, London B & Nerbonne JM (1999). Molecular basis of transient outward K^+ current diversity in mouse ventricular myocytes. *J Physiol* **521**, 587–599.

Gutman GA, Chandy KG, Grissmer S, Lazdunski M, Mckinnon D, Pardo LA, Robertson GA, Rudy B, Sanguinetti MC, Stuhmer W & Wang X (2005). International Union of Pharmacology. LIII. Nomenclature and molecular relationships of voltage-gated potassium channels. *Pharmacol Rev* **57**, 473–508.

Hasdemir B, Fitzgerald DJ, Prior IA, Tepikin AV & Burgoyne RD (2005). Traffic of Kv4 K^+ channels mediated by KChIP1 is via a novel post-ER vesicular pathway. *J Cell Biol* **171**, 459–469.

Johns DC, Marx R, Mains RE, O'Rourke B & Marban E (1999). Inducible genetic suppression of neuronal excitability. *J Neurosci* **19**, 1691–1697.

Kislauskis EH, Li Z, Singer RH & Taneja KL (1993). Isoform-specific 3′-untranslated sequences sort α-cardiac and β-cytoplasmic actin messenger RNAs to different cytoplasmic compartments. *J Cell Biol* **123**, 165–172.

Kuo HC, Cheng CF, Clark RB, Lin JJ, Lin JL, Hoshijima M, Nguyen-Tran VT, Gu Y, Ikeda Y, Chu PH, Ross J, Giles WR & Chien KR (2001). A defect in the Kv channel-interacting protein 2 (KChIP2) gene leads to a complete loss of I_{to} and confers susceptibility to ventricular tachycardia. *Cell* **107**, 801–813.

Li H, Guo W, Yamada KA & Nerbonne JM (2004). Selective elimination of $I_{K,slow1}$ in mouse ventricular myocytes expressing a dominant negative Kv1.5 α subunit. *Am J Physiol Heart Circ Physiol* **286**, H319–328.

Liu J, Kim K-H, London B, Morales M & Backx P (2011). Dissection of the voltage-activated potassium outward currents in adult mouse ventricular myocytes: $I_{to,f}$, $I_{to,s}$, $I_{K,slow1}$, $I_{K,slow2}$, and I_{ss}. *Basic Res Cardiol* **106**, 189–204.

London B, Guo W, Pan X, Lee JS, Shusterman V, Rocco CJ, Logothetis DA, Nerbonne JM & Hill JA (2001). Targeted replacement of KV1.5 in the mouse leads to loss of the 4-aminopyridine-sensitive component of $I_{K,slow}$ and resistance to drug-induced QT prolongation. *Circ Res* **88**, 940–946.

London B, Wang DW, Hill JA & Bennett PB (1998). The transient outward current in mice lacking the potassium channel gene Kv1.4. *J Physiol* **509**, 171–182.

Marionneau C, Brunet S, Flagg TP, Pilgram TK, Demolombe S & Nerbonne JM (2008). Distinct cellular and molecular mechanisms underlie functional remodeling of repolarizing K^+ currents with left ventricular hypertrophy. *Circ Res* **102**, 1406–1415.

Marionneau C, Townsend RR & Nerbonne JM (2011). Proteomic analysis highlights the molecular complexities of native Kv4 channel macromolecular complexes. *Semin Cell Dev Biol* **22**, 145–152.

Mitchell GF, Jeron A & Koren G (1998). Measurement of heart rate and Q-T interval in the conscious mouse. *Am J Physiol* **274**, H747–H751.

Nerbonne JM (2011). Repolarizing cardiac potassium channels: multiple sites and mechanisms for CaMKII-mediated regulation. *Heart Rhythm* **8**, 938–941.

Nerbonne JM & Kass RS (2005). Molecular physiology of cardiac repolarization. *Physiol Rev* **85**, 1205–1253.

Niwa N & Nerbonne JM (2010). Molecular determinants of cardiac transient outward potassium current (I_{to}) expression and regulation. *J Mol Cell Cardiol* **48**, 12–25.

Niwa N, Wang W, Sha Q, Marionneau C & Nerbonne JM (2008). Kv4.3 is not required for the generation of functional $I_{to,f}$ channels in adult mouse ventricles. *J Mol Cell Cardiol* **44**, 95–104.

Norris AJ, Foeger NC & Nerbonne JM (2010*a*). Interdependent roles for accessory KChIP2, KChIP3, and KChIP4 subunits in the generation of Kv4-encoded I_A channels in cortical pyramidal neurons. *J Neurosci* **30**, 13644–13655.

Norris AJ, Foeger NC & Nerbonne JM (2010*b*). Neuronal voltage-gated K^+ (Kv) channels function in macromolecular complexes. *Neurosci Lett* **486**, 73–77.

Petrecca K, Miller DM & Shrier A (2000). Localization and enhanced current density of the Kv4.2 potassium channel by interaction with the actin-binding protein filamin. *J Neurosci* **20**, 8736–8744.

Pioletti M, Findeisen F, Hura GL & Minor DL, Jr (2006). Three-dimensional structure of the KChIP1–Kv4.3 T1 complex reveals a cross-shaped octamer. *Nat Struct Mol Biol* **13**, 987–995.

Pongs O & Schwarz JR (2010). Ancillary subunits associated with voltage-dependent K^+ channels. *Physiol Rev* **90**, 755–796.

Radicke S, Cotella D, Graf EM, Banse U, Jost N, Varro A, Tseng G-N, Ravens U & Wettwer E (2006). Functional modulation of the transient outward current I_{to} by KCNE β-subunits and regional distribution in human non-failing and failing hearts. *Cardiovasc Res* **71**, 695–703.

Radicke S, Cotella D, Graf EM, Ravens U & Wettwer E (2005). Expression and function of dipeptidyl-aminopeptidase-like protein 6 as a putative β-subunit of human cardiac transient outward current encoded by Kv4.3. *J Physiol* **565**, 751–756.

Roepke TK, Kontogeorgis A, Ovanez C, Xu X, Young JB, Purtell K, Goldstein PA, Christini DJ, Peters NS, Akar FG, Gutstein DE, Lerner DJ & Abbott GW (2008). Targeted deletion of *kcne2* impairs ventricular repolarization via disruption of $I_{K,slow1}$ and $I_{to,f}$. *FASEB J* **22**, 3648–3660.

Shaner NC, Campbell RE, Steinbach PA, Giepmans BN, Palmer AE & Tsien RY (2004). Improved monomeric red, orange and yellow fluorescent proteins derived from *Discosoma* sp. red fluorescent protein. *Nat Biotechnol* **22**, 1567–1572.

Shibata R, Misonou H, Campomanes CR, Anderson AE, Schrader LA, Doliveira LC, Carroll KI, Sweatt JD, Rhodes KJ & Trimmer JS (2003). A fundamental role for KChIPs in determining the molecular properties and trafficking of Kv4.2 potassium channels. *J Biol Chem* **278**, 36445–36454.

Stuhmer W, Ruppersberg JP, Schroter KH, Sakmann B, Stocker M, Giese KP, Perschke A, Baumann A & Pongs O (1989). Molecular basis of functional diversity of voltage-gated potassium channels in mammalian brain. *EMBO J* **8**, 3235–3244.

Sun X & Wang H-S (2005). Role of the transient outward current (I_{to}) in shaping canine ventricular action potential – a dynamic clamp study. *J Physiol* **564**, 411–419.

Thomsen MB, Sosunov EA, Anyukhovsky EP, Özgen N, Boyden PA & Rosen MR (2009*a*). Deleting the accessory subunit KChIP2 results in loss of $I_{to,f}$ and increased $I_{K,slow}$ that maintains normal action potential configuration. *Heart Rhythm* **6**, 370–377.

Thomsen MB, Wang C, Ozgen N, Wang H-G, Rosen MR & Pitt GS (2009*b*). The accessory subunit KChIP2 modulates the cardiac L-type calcium current. *Circ Res* **104**, 1382–1389.

Wang H, Yan Y, Liu Q, Huang Y, Shen Y, Chen L, Chen Y, Yang Q, Hao Q, Wang K & Chai J (2007). Structural basis for modulation of Kv4 K^+ channels by auxiliary KChIP subunits. *Nat Neurosci* **10**, 32–39.

Xu H, Barry DM, Li H, Brunet S, Guo W & Nerbonne JM (1999*a*). Attenuation of the slow component of delayed rectification, action potential prolongation, and triggered activity in mice expressing a dominant-negative Kv2 α subunit. *Circ Res* **85**, 623–633.

Xu H, Guo W & Nerbonne JM (1999*b*). Four kinetically distinct depolarization-activated K^+ currents in adult mouse ventricular myocytes. *J Gen Physiol* **113**, 661–678.

Competing interests

None.

Author contributions

All experiments were performed in the laboratory of J.M.N. N.C.F. contributed to the conception and design of the experiments, the collection, analysis and interpretation of data and to writing the manuscript. W.W. contributed to the design of the experiments, as well as to the collection, analysis and interpretation of data. R.L.M. contributed to the collection, analysis and interpretation of data. J.M.N. contributed to the conception and design of the experiments, the interpretation of data and to writing the manuscript. All authors have contributed through critical review of the intellectual content of the manuscript and all have approved the submitted version.

Funding

We acknowledge the financial support provided by the National Institutes of Health (HL034161 to J.M.N.); N.C.F. was supported by an institutional training grant (T32-HL007275) from the National Heart Lung and Blood Institute.

Acknowledgements

We thank Dr Joshua Sanes for the gift of the pSV/Lox-neo-lox targeting vector, Dr Roger Tsien for the gift of the tdTomato fluorophore construct, Dr David Johns for the gift of the adenovirus shuttle construct, Ms Amy Huntley for assistance in preparing cortical protein samples and Mr Rick Wilson for the maintenance and screening of mice. We would also like to thank Drs Kai-Chien Yang, Scott Marrus and Yarimar Carrasquillo for many valuable discussions and for comments on the manuscript.